Dynamic behaviour of adobe bricks in compression

The role of fibres and water content at various loading rates

Li Piani, T.; Weerheijm, J.; Peroni, M.; Koene, L.; Krabbenborg, D.; Solomos, G.; Sluys, L. J.

DOI
10.1016/j.conbuildmat.2019.117038

Publication date
2020

Document Version
Final published version

Published in
Construction and Building Materials

Construction and Building Materials 230 (2020) 117038

Contents lists available at ScienceDirect

Construction and Building Materials

journal homepage: www.elsevier.com/locate/conbuildmat

Dynamic behaviour of adobe bricks in compression: The role of fibres and water content at various loading rates

T. Li Piani [a,b,c,*], J. Weerheijm [a,c], M. Peroni [d], L. Koene [b], D. Krabbenborg [b], G. Solomos [d], L.J. Sluys [a]

[a] TU Delft, Stevinweg 1, 2628 CN Delft, The Netherlands
[b] NLDA – Faculty of Military Sciences, NL-1781 CA Den Helder, The Netherlands
[c] TNO – Defence, Safety and Security, 2280 AA Rijswijk, The Netherlands
[d] European Commission – Joint Research Centre (JRC), 21027 Ispra, Italy

HIGHLIGHTS

- Comprehensive characterization of adobe material at a wide range of strain rates.
- Quali-quantitative role of interstitial water in adobe in statics and dynamics.
- Quali-quantitative role of mixing fibers in adobe in statics and dynamics.
- Constitutive modelling of adobe including DIF functions in dynamics.

ARTICLE INFO

Article history:
Received 13 March 2019
Received in revised form 14 September 2019
Accepted 17 September 2019

Keywords:
Adobe
Dynamics
Hopkinson bar
Strain rate
Brick
Fiber
Soil
Water
Dynamic increase factor

ABSTRACT

This paper presents the results of an experimental research aimed at assessing the material performance of adobe bricks in compression for a wide range of induced strain rates, from statics to high velocity impact. Adobe connotes a traditional masonry whose bricks are made of sundried soil mixtures possibly reinforced with natural fibres and joined together using mud mortar. The inclusion of fibre and the presence of water in the mixture have a dominant effect on the mechanical performance of adobe bricks and masonry. Their influence on the dynamic behaviour of this material is quantified and interpreted in this study at high strain rates also with data produced through Hopkinson bar testing. Appropriate dynamic increase factors and constitutive equations for adobe materials in dynamics are also investigated. The paper presents the experimental campaign, shows the main results and offers qualitative and quantitative interpretations for the principal damage patterns observed.

1. Introduction

Contemporary society is confronted with many threats of different nature, from international terrorism to environmental emergency. Safety and protection of critical buildings and infrastructures are among the top priorities of governments around the world including the European Commission and its Joint Research Centre [1]. In Europe terrorist attacks have recently involved targets within the domain of the city, inside or in the proximity of dwellings and infrastructure for civilian use [2]. In this context, strategies of strengthening of the target [3] are neither economically nor socially sustainable. Thus, built infrastructure nowadays must be made resilient through the design process with respect to a wide range of dynamic loadings which not only include natural hazards such as floods and earthquakes, but also impacts and explosions as man-made threats [4]. These dynamic phenomena, with different intensity, are characterized by higher deformation rates imposed to the material with respect to static loadings [5].

Many civilian buildings and constructions are mainly made of brittle materials, such as concrete, ceramics, glass and rocks [6]. The properties of these materials are sensitive to the rate of loading and their physical-mechanical behaviour changes according to the imposed loadings [7]. If assuming static properties within the

* Corresponding author at: TU Delft, Stevinweg 1, 2628 CN Delft, The Netherlands.
E-mail address: t.lipiani@tudelft.nl (T. Li Piani).

https://doi.org/10.1016/j.conbuildmat.2019.117038
0950-0618/

design process may constitute a known approximation with respect to seismic loadings, using the same approach with regards to strain rates corresponding to impacts and blasts may lead to serious errors in the prediction of structural damage and fragmentation effects [8,9].

These dynamic loadings require also the adoption of appropriate constitutive models capable of addressing the changes in the response of the material to high strain rates [6]. In order to incorporate these effects in analytical and numerical models, it is of paramount importance to experimentally characterize the material performance at all relevant deformation rates [5].

The study of the dynamic properties of cement-based materials has been consolidated over the last fifty years. It is generally accepted that strength of concrete increases with strain rate [10]. However, not all typical features related to the dynamic response of the material have been clarified and interpreted yet [11]. On the other hand, very limited sources of knowledge concern building materials for masonry constructions such as clay or stone, despite being of paramount importance for a reliable design of masonry [9–13]. If this is true for modern bricks and mortar, the state of knowledge is even more limited with regards to traditional masonry building materials, such as adobe [14].

Adobe connotes a traditional masonry whose bricks are made of raw mixtures of clay, sand and silt. Soil is mixed with natural fibres in the field according to local availability of resources and cast in moulds to be sundried according to building traditions. After air curing, bricks are joined together using mud mortar. Adobe constitutes one of the first forms of masonry on earth [15]. More than one third of the world population still lives in earthen dwellings, which constitute 10% of the built heritage [16]. Unfortunately, these structures are spread in areas of the world prone to earthquakes or involved into military operations, with severe numbers of human losses and built heritage disruption every year [17,18]. Moreover, despite the presence of many examples of this building technique in Europe, the production and use of adobe materials have declined after the industrial revolutions in today's building industry [19].

Two critical factors threaten more than others built heritage of adobe and limit its use in current practice. These threats are its low strength and durability properties [20]. These effects are directly linked to the material selection and production processes inherent to adobe masonry. They result from common practices adopted for adobe in the field while their implications on the material properties are not standardized and scarcely addressed in literature [20]. For instance, avoiding industrial baking processes makes the material properties dependent on the water content in the mixture over its life cycle [21]. Furthermore, bricks and mortar are still often produced mixing soil with organic content locally available, regardless of the mineralogical properties of soil elements and the chemical interactions with fibers and water. Instead, a proper characterization of adobe must address the influence of such inclusions on the microstructure of the resulting component of the adobe masonry.

Addressing the role that fibers and water contents in soil mixtures play on the mechanical material properties is of paramount importance because these are among the features which configure adobe as a eco-friendly building material [22]. Natural fibres improve the thermal and acoustic properties of adobe [16]. Traditional production and construction processes are characterized by limited costs and minimum carbon footprint with respect to industrial products. For these reasons, natural fibres or binders and traditional drying processes have been recently applied also in modern building materials such as concrete and clay [23–25]. Therefore, assessing the influence of fibres and drying processes on the properties of adobe is crucial in a global perspective.

This paper presents an experimental and numerical study of the material performance of bricks of traditional adobe at a wide range of strain rates. It addresses the effects on the material behaviour of low (statics), intermediate and high strain rates. High strain rates on the material are simulated using Hopkinson bar tests. The influence of water content and fiber contained in the mixture on the material performance is addressed and interpreted both in statics and dynamics.

In the following paragraphs, the experimental campaign is described and its results are reported. Observed effects of strain rates, fiber and water contents on the mechanical performance of adobe are described and dynamic increase factors are quantified in Section 3. These observations are further interpreted in Section 4.

2. The experimental campaign

A joint experimental campaign including Delft University of Technology (TU Delft), TNO, Dutch Ministry of Defence and the Joint Research Centre of the European Commission, was carried out in 2018.

The investigation was aimed to characterize the physical and mechanical performance of components of adobe masonry loaded in compression at a wide range of strain rates corresponding to induced loadings ranging from statics to the ones corresponding to earthquakes and impacts [26].

The influence of fibre reinforcement and water content in the soil mixture on the material properties for each strain rate was aimed to be quantified and evaluated.

2.1. Materials

Two types of adobe bricks were selected for testing. They resulted from the same soil selection but only one of them contained substantial percentages of natural fibres.

Cylindrical samples of about 40 mm in diameter with unitary slenderness were drilled from both bricks types and basal surfaces were rectified to achieve parallel planes with a tolerance of 0.1 mm (Fig. 1). 40 mm is the minimum size required for static testing on masonry components in codes [27] and it was considered as sufficiently large to represent the average heterogeneous structure of adobe in this campaign. Shape and size were chosen also to limit radial confinement due to inertia during the Hopkinson bar tests which is found to be proportional to the cross sectional area, while assuring equilibrium along the height, which is usually assured for low slenderness [9].

Each type of adobe was tested at two different water contents in the mixture. Air dried samples were air cured for 28 days at

(a) (b)

Fig. 1. Example of tested fiber free (a) and fiber reinforced (b) adobe.

laboratory conditions while fully dried samples were further baked in the oven.

2.2. Test setup and methods

Physical characterization tests were performed at the laboratory of soil mechanics and geo-engineering of the Delft University of Technology. Mechanical tests were performed at the European Laboratory for Structural Assessment (ELSA) of the Joint Research Centre in Ispra, Italy.

2.2.1. Physical tests

Granulometric composition of the tested adobe was determined on three samples per type according to standard BS 1377-2 [28]. Density and moisture content at laboratory conditions were determined on fifteen samples per type according to NT Build 333 [29]. However, the prescribed temperature of 105 °C for the oven-drying process was lowered to 85 °C, in order to prevent damage in the micro-structure, which is found to happen in cementitious materials for temperatures higher than 100 °C [30]. In fact, samples subjected to moisture content and density tests were also used for mechanical tests. The complete drying process was considered to be achieved when in two subsequent measurements, the variation in mass was lower than 1 g. Three days were needed in average to fully dry adobe samples.

2.2.2. Static tests

Static tests were performed on five samples per type and drying conditions. Tests were performed using an MTS universal testing machine (810 Material Testing System-50 kN). Two special compression platens (of 115 mm in diameter) were used to correctly load the specimens in compression. Displacement controlled tests at a constant velocity of 0.01 mm/s were performed. Corresponding strain rates ($\dot{\epsilon}_1$) were calculated as the ratio between applied deformation rate and specimen height. Average strain rates of about 3 $10^{-4}\,s^{-1}$ with negligible standard deviation ($2.81 \pm 0.01\ \ 10^{-4}\,s^{-1}$) were produced. Displacement and forces were recorded by a FlexTest 40 Digital controller unit. Average stress-strain plots were derived normalizing each curve over the corresponding cross section areas and heights. A camera was installed to acquire high resolution photo sequences at 1 frames/s synchronized with the sensors data recorded by the

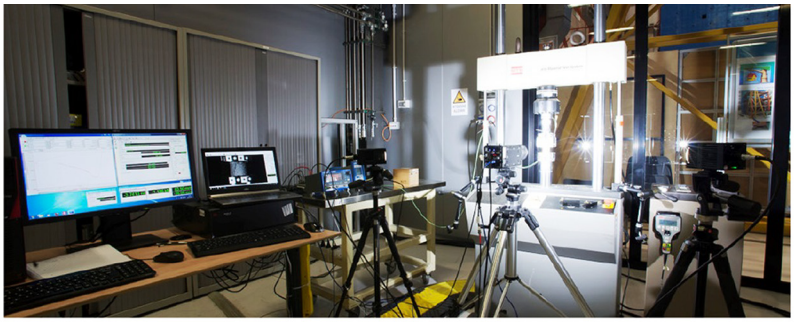

(a)

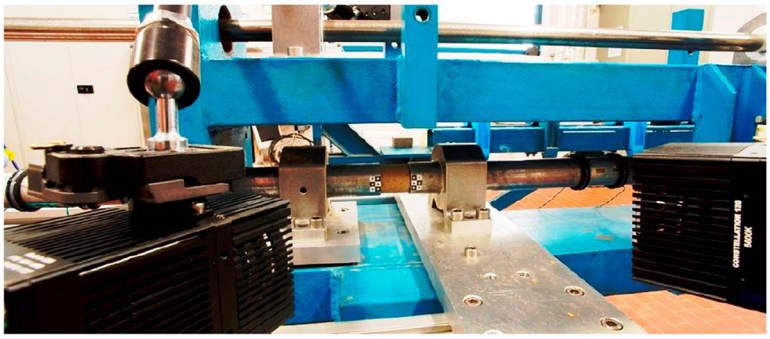

(b)

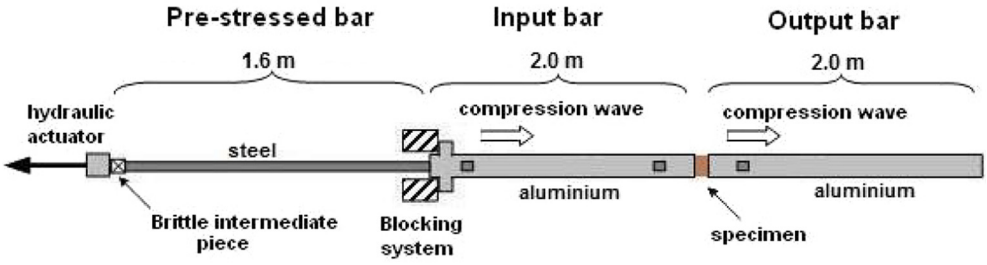

(c)

Fig. 2. Setup of servo-hydraulic machine tests (a); Detail of Hopkinson bar in front of the specimen (b); Schematic picture of the JRC modified Hopkinson test setup for compression (c).

testing machine at sample rate of 10 Hz. Test setup is shown in Fig. 2(a).

2.2.3. Dynamic tests

Dynamic tests were performed at two different strain rates, in the range corresponding to impacts and blasts [26]. Five tests per type and drying conditions were performed. Tests at an intermediate strain rate were performed using the same setup and machine of Fig. 2(a), with two differences. Displacement controlled tests were performed at approximately 100 mm/s. Corresponding strain rates of about 3 s^{-1} ($\dot{\epsilon_2}$) with negligible deviation (2.89 ± 0.01 s^{-1}) were produced. Force and displacement signals have been recorded (at a sample-rate of 20 kHz) using a National Instruments acquisition board (NI USB-6366) controlled with the Labview software and photo sequences were recorded at 5000 frames/s with a Photron SA1.1 high speed camera. At both strain rates in dynamics, average stress-strain plots were derived normalizing each curve of response over the corresponding cross section areas and heights.

Strain rates of the order of hundreds s^{-1} can be obtained only using specific setup and machines, namely drop hammer machines or split Hopkinson bars. A modified Hopkinson bar at the Hop-Lab of JRC was used to test adobe at high strain rates. The input and output bars of 40 mm diameter are made of aluminium. The input pulse was generated through the pre-stressing and abrupt release of a steel portion of the bar of 25 mm in diameter. Test setup is shown in Fig. 2(b). A scheme of the machine provided with geometrical information is graphically reported in Fig. 2(c). For a detailed report of the dynamic test machine, the reader is referred to [31,14]. In the tests, the incident bar applied a constant velocity of about 4200 mm/s to the sample. Resulting strain rates $\dot{\epsilon_3}$ of about 120 s^{-1} with negligible deviation (119.1 ± 1.3 s^{-1}) were determined. For each test, specimen loading conditions and corresponding bar ends displacements were calculated by properly processing the strain signals record with a chain of semiconductor strain gages applied on the bars. For this purpose, a sample-rate of 5 MHz was used and the data acquisition system GAGE Module A/D Express CSE8482-H2 with dedicated software was employed. For each test, a thin layer of vaseline was applied at the interfaces between the bar end and the sample surfaces to minimize friction and maximise plane-parallelism. Moreover, samples were pre-stressed up to 5% of the static strength for clamping and horizontal positioning purposes. Time-syncronized high-resolution videos were recorded at 50,000 frames/s using the Photron SA1.1 digital camera. Image resolution is adequate to track failure patterns also in case of high velocity impacts.

2.3. Elaboration of results

2.3.1. Physical tests

The mean curve of the soil granulometry distribution of the tested adobe is shown in Fig. 3(a). The volume percentages ranges of soil elements are reported in Table 1 according to particle sizes (2–0.06 mm sand; 0.06–2 μm silt; <2 μm clay). The soil of the tested adobe is defined as a clayey sandy silt. The percentages of organic content are also included in the table. Soil of Type B contains a mixture of wooden and straw fibers of different sizes and shapes (maximum dimension of 20 mm (Fig. 3b)). Traces of organic content were also found in Type A.

The average densities of the two types of adobe differ significantly, whereas their moisture content at laboratory conditions after 28 days of air curing shows similar values (Table 1).

2.3.2. Static tests

Failure of cylindrical samples in compression is characterized by a mixed cracking pattern with parallel and diagonal cracks with respect to the loading direction. Cracks start from random points of the sample spreading irregularly over the surface. The first cracks appear before the attainment of the maximum load. In case of fibre free samples, this occurs at an earlier stage (0.85 of the strain corresponding to peak load in average) with respect to the fibre enriched samples (0.93). Typical crack distributions and their progression are shown through snap shots in Figs. 4 and 5 for both types at different deformation stages (first rows). Samples from Type B are characterized by more diffuse and less visible cracks. These often follow the visible fibre orientation. Moreover, fibre reinforced samples show significantly larger lateral volume expansion, remaining coherent until larger displacements (Fig. 6(b, c)). These trends do not change if samples are fully dried. However, for both types, in oven dried specimens the first crack in average appears at higher load levels (0.91 of peak for Type A and 0.97 for Type B) and they tend to be slightly less spread (Fig. 7(a–c)).

Mean stress strain plots are shown from Fig. 6a by averaging test quantities over height and cross section areas of the specimen (Par. 2.2.2). Despite common practice, it should be noted that this is rigorous only when deformations in the post peak part of the curve are not too localized [32]. Values of key material parameters in compression were derived from each curve. They are the compressive strength f_b, the corresponding critical strain ϵ_{f_b} and the elastic modulus E (meant as chord modulus between 5% and 33% of compressive strength). Moreover, an ultimate deformation value ϵ_u, meant as the strain corresponding to 20% decay of the maximum load was calculated to characterize the early post peak deformation capacity [33]. In static (as well as in dynamic tests), possible outliers were excluded using the Interquartile Range Method and no more than one test was excluded for each type and drying condition. Average values and related standard deviations are listed in Table 2. Mean stress strain curves are shown for both adobe types and drying conditions in Fig. 8. A modest scatter (more pronounced for Type B) characterizes the curves of both types which is typical scatter associated to adobe in literature (Fig. 9a) [20]. Four different regions are distinguished in all curves of response. A nonlinear initial phase (“1” in Fig. 8(a, b)) is followed by a dominant linear elastic region (2). A second pre-peak non linearity (3) precedes the attainment of the peak load, which is followed by a softening branch (4). In fibre reinforced samples, larger extensions of the pre-peak non linear phases in the stress-strain are observed with respect to fibre free and the degradation of the softening curve occurs at a significantly lower rate (Fig. 8b). This corresponds to an enhanced ductility associated to Type B in terms of critical strain (order of 1:3) and ultimate strain (order of 1:4). On the contrary, the mechanical performance of fibre free samples is higher both in terms of compressive strength (order 1:2) and elastic modulus (order of 1:3).

The depicted trends in the shape of stress curves and corresponding relationships among types do not change if samples are oven dried (Fig. 8(a, b)). For both, fully dried samples show higher strength (order of 1:2) and higher Young’s modulus (Fig. 7(a–c)). However, the influence on parameters regarding deformation is negligible (Table 2).

2.3.3. Dynamic tests

Also in dynamics, failure pattern of adobe samples is characterized by the development of parallel-diagonal patterns of cracks (Figs. 4 and 5, second and third rows). However, the first cracks have systematically a more straight orientation than in statics. This is particularly the case for fibre free samples, while a more diffuse and random initial crack pattern remains associated to Type B as in statics (Fig. 6, second and third rows). For both types and drying conditions, damage initiation processes appear visible in cylinders at later deformation stages of the dynamic curves of response. This

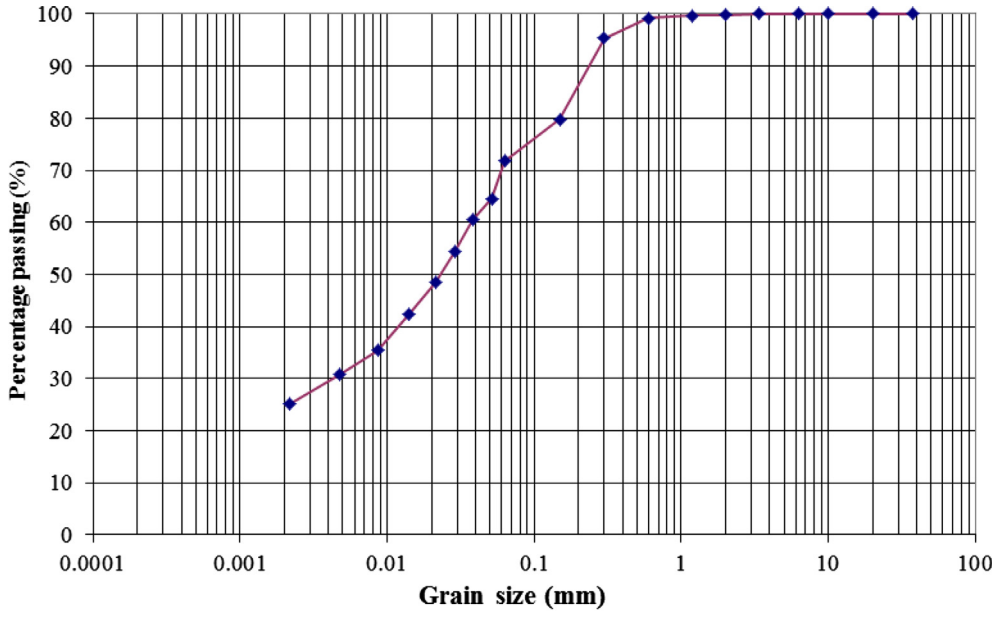

(a)

(b)

Fig. 3. Typical soil granulometric distribution (a) and microscopic image zoom on fiber reinforcement (b) of the tested adobe.

Table 1
Ranges of percentages of soil elements and fiber content by weight for the tested adobe and mean values (and standard deviations) for dry density and water content.

Type	Soil Granulometry				Density	Water content
	% Clay	% Silt	% Sand	%bw Fiber	kg/m^3	%
A	24–25	47–48	27–28	<2	1790 (12)	2.3 (0.2)
B	24–25	47–48	27–28	17–18	1180 (20)	2.4 (0.2)

is valid also comparing results from the intermediate and the high strain rate tests. On air dried samples, the first crack appears just at peak load for $\dot{\epsilon}_2$ (0.95 of the critical strain for Type A and 0.99 for Type B) and in softening for $\dot{\epsilon}_3$ (1.06 for Type A and 1.12 for Type B). However, more severe damage characterizes the sample response at large deformation levels in softening. Fragmentation and pulverization occur in the softening phase. This is particularly the case for Type A.

Considering dynamic tests separately at each strain rate, the regions which compose the stress-deformation curves correspond to those observed in statics (Fig. 8(c, d)). As in statics, for each rate the tests on fibre reinforced samples show enhanced ductility and smoother curves than the corresponding fibre free tests, which in turn are characterized by higher values of strength and elastic modulus. For both types, oven drying does not change the failure pattern while it improves the strength parameters as observed in 2.3.2 (Fig. 7, second and third rows).

Analysing each type and drying condition at all the strain rates tested, it emerges that the values associated to the main key material properties change in dynamics (Table 2). In the following, the effects of strain rate on material properties are quantified in terms of mean dynamic increase factors (DIF), the ratios between the value for the dynamic and the static property [34]. Mean values are shown as a log-scale function of the applied strain rate in Fig. 10 and 11 and standard deviations are included in symbol thickness [35]. The validity of the essential assumption of stress

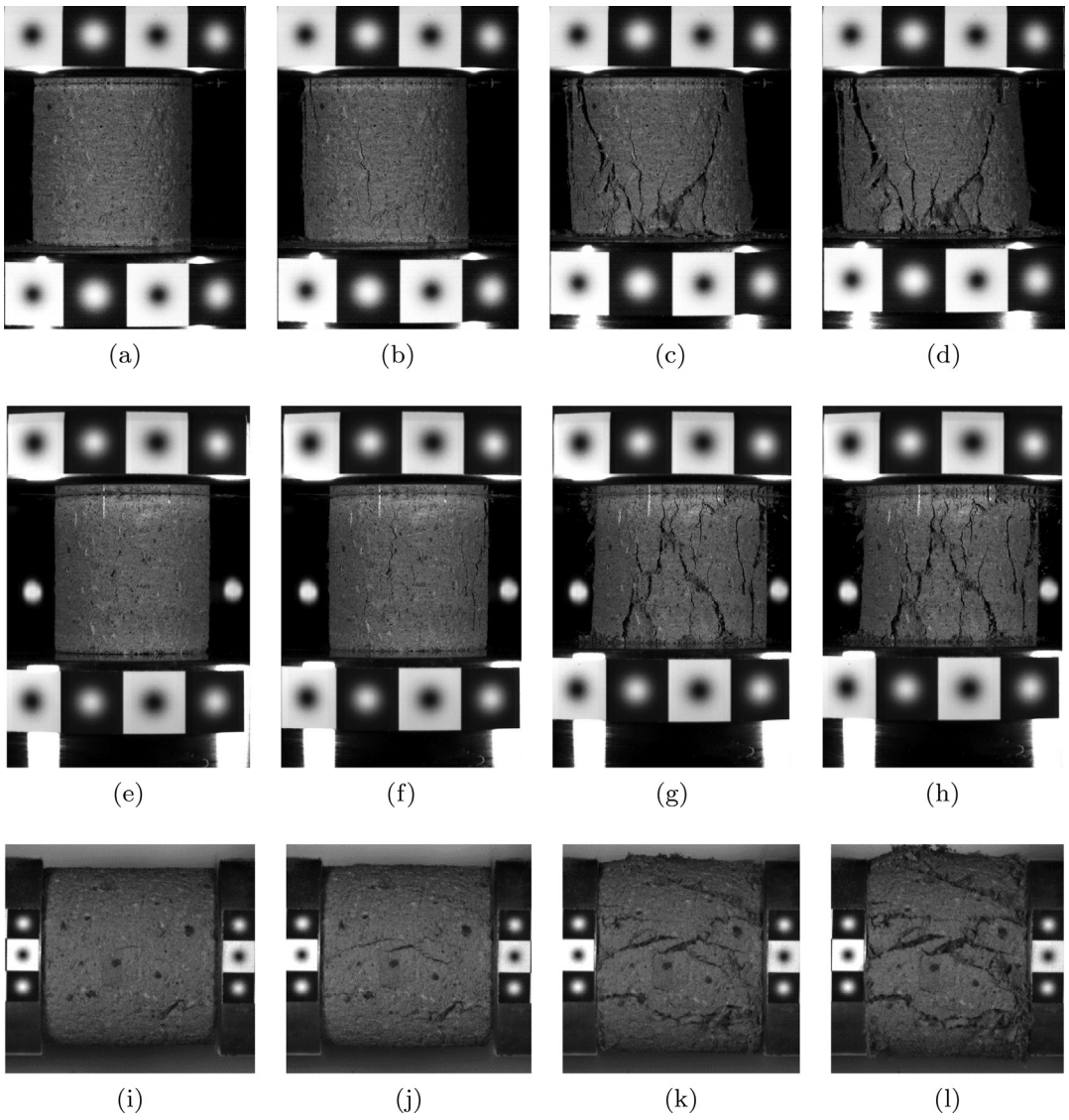

Fig. 4. Comparison of typical damage progression for air dried Type A, at first crack appearance and 4%, 8%, 10% strain levels for static test (first row), intermediate strain rate test (second row) and split Hopkinson bar test (third row).

equilibrium in the specimen during split Hopkinson bar tests has been checked and calculated average relative errors of the order of 5% in the non linear force equilibrium conditions were considered as acceptable (Fig. 9b). For all tests it counts that the ratio of the difference in forces and the average force did not exceed 0.1 for the response regions 2 and 3 (Fig. 8).

For both types and drying conditions, all tests in dynamics reveal higher values for the compressive strength with respect to the corresponding static ones. This trend is not linear: higher ratios are associated to results of split Hopkinson bar tests (Fig. 10). The rate of increment is lower for samples reinforced with fibres. This happens for both strain rates with similar proportions. For both types, air dried samples show a strength increase proportionally larger if compared with corresponding oven dried samples (Fig. 10a). The maximum *DIF* is associated to air dried type A samples (1.84 at high rate) and the lowest to oven dried type B samples (1.66).

Similar trends denote the sensitivity to rate on adobe in terms of elastic modulus at high rates (Fig. 10b). The maximum rate effect is of the same order of magnitude as for compressive strength (1.73). Similarly, the dynamic increase is the largest for the air dried fibre free adobe and the lowest for oven dried fibre reinforced samples (1.40). Negligible sensitivity to the rate is associated to the initial tangent stiffness (Fig. 7(a, d, g)).

Higher uncertainty concerns the assessment of the influence of rate on the deformation parameters. In general, the ductility parameters are characterized by a minimal rate effect with respect to the performance in strength and not always consistent trends characterize results for Type A and Type B (Fig. 11). Critical strain is slightly larger than in statics for fibre-free samples (*DIF* of 1.09) at intermediate strain rate. A slight reduction is shown by fibre reinforced matrix (0.96) for the same loading. For both, the critical strain more clearly decays in Hopkinson bar tests in a similar range for both types included between 0.81 (Type B) and 0.77 (Type A). Variation in the softening parameter is minimal for all dynamic tests (Fig. 11b). For both parameters of deformation, the rate of enhancement does not change if samples are oven dried (Fig. 11).

3. Analysis of results: addressing a constitutive model for Adobe in statics and dynamics

As for cement-based materials, the mechanical parameters of the tested adobe show sensitivity to the applied rate of loading. In concrete, rate sensitivity in dynamics is usually measured in

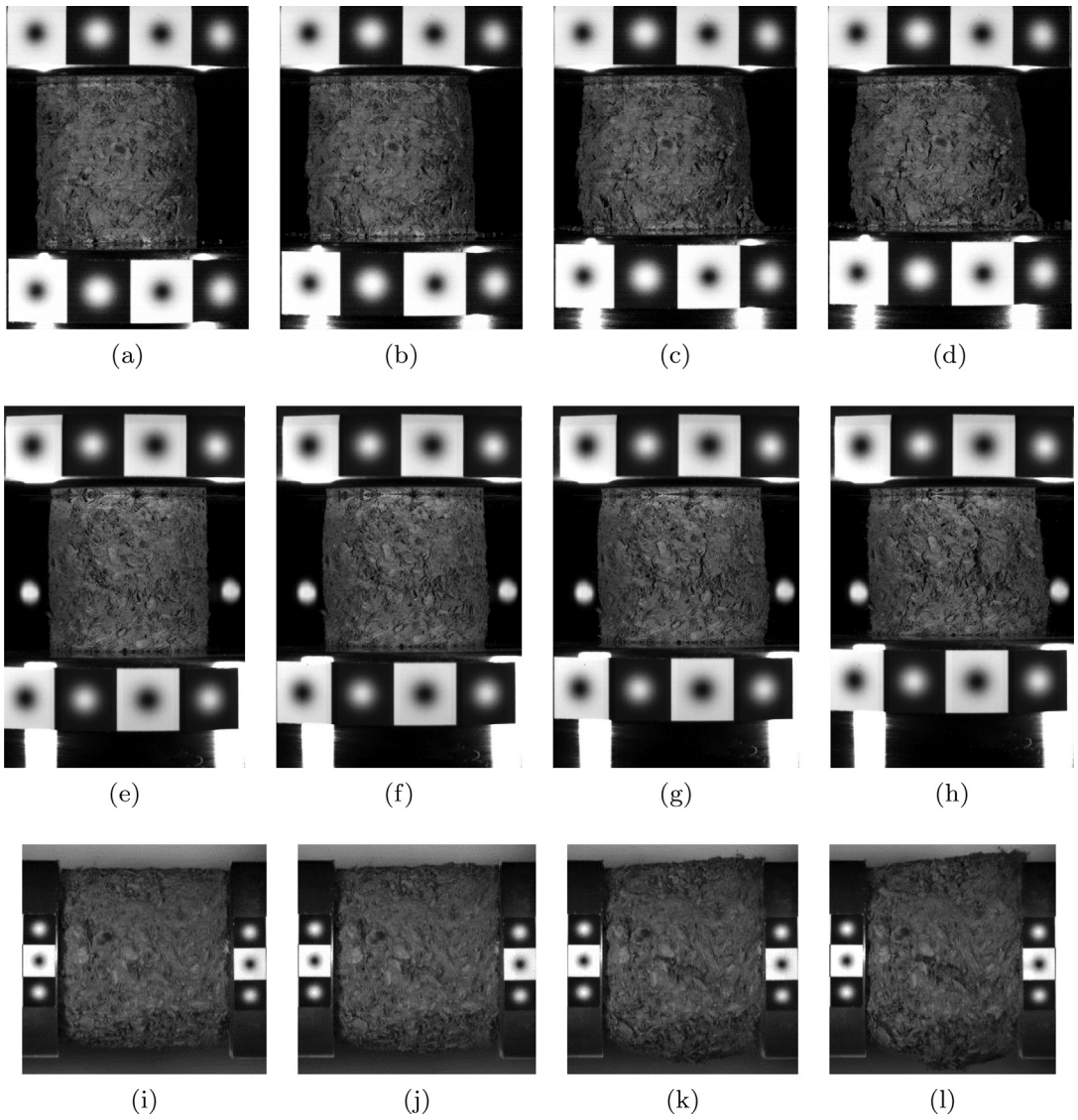

Fig. 5. Comparison of typical damage progressions for air dried Type B at first crack appearance and 8%, 12%, 15% strain levels for static test (first row), intermediate strain rate test (second row) and split Hopkinson bar test (third row).

terms of strength enhancement ratio. Its dynamic increase factor is usually higher in tension than in compression [30]. In compression strength can increase up to three times [9] and guidelines suggest to consider an increment of 85% in the design for impact loadings for ordinary concrete subjected to high strain rates [26]. For the tested adobe material, rate sensitivity in strength is slightly less pronounced than reported for concrete. This is in agreement with the only other source of information available in literature regarding impact tests on adobe at high strain rates (Fig. 12) [14,36]. In Fig. 12 dynamic increase factors for adobe lie on the lower boundary of the cloud of data usually associated to concrete [26]. This is especially valid for strain rate $\dot{\epsilon_3}$ (split Hopkinson bar tests).

The enhancement of the strength in compression can be addressed in dynamics using rate dependent functions. Many different formulations have been proposed in literature for a wide range of cementitious materials [34,9]. They are usually implemented into numerical models to simulate the mechanical response under highly dynamic loadings [37,12].

In order to address the increase in the compressive strength of quasi brittle materials at high rates, the most commonly adopted formulations are log-log power functions. The most comprehensive and widely accepted reference to design the compressive strength of normal concrete ($f_b \leqslant 50$ MPa) in dynamics is the CEB-FIB model [38]. It defines DIF as:

$$\begin{cases} DIF. = \left(\frac{\dot{\epsilon}}{\dot{\epsilon}_s}\right)^{1.026\alpha} for\, \dot{\epsilon} \leqslant 30\ s^{-1} \\ DIF. = \gamma\left(\frac{\dot{\epsilon}}{\dot{\epsilon}_s}\right)^{0.33} for\, \dot{\epsilon} \geqslant 30\ s^{-1} \end{cases} \quad (1)$$

where $\dot{\epsilon}$ is the current strain rate in dynamics, $\dot{\epsilon}_s$ is the reference static strain rate (equal to 3 10^{-5}) and:

$$\begin{cases} \alpha = \frac{1}{5+9\left(\frac{f_b}{f_{bo}}\right)} \\ \gamma = 10^{6.156\alpha-2} \end{cases} \quad (2)$$

where f_{bo} is a reference strength of 10 MPa. Fig. 13 shows the CEB model for a concrete of 30 MPa of strength. It matches relatively well with experimental data on concrete. However, it clearly overestimates rate dependency of adobe, represented by average plots and standard deviations associated to air dried Type A and Type B (Fig. 12). Other log-log functions proposed in literature for concrete, mortar and clay also overestimate the dynamic performance of adobe [9–13,39]. The overestimation is also enhanced if the values

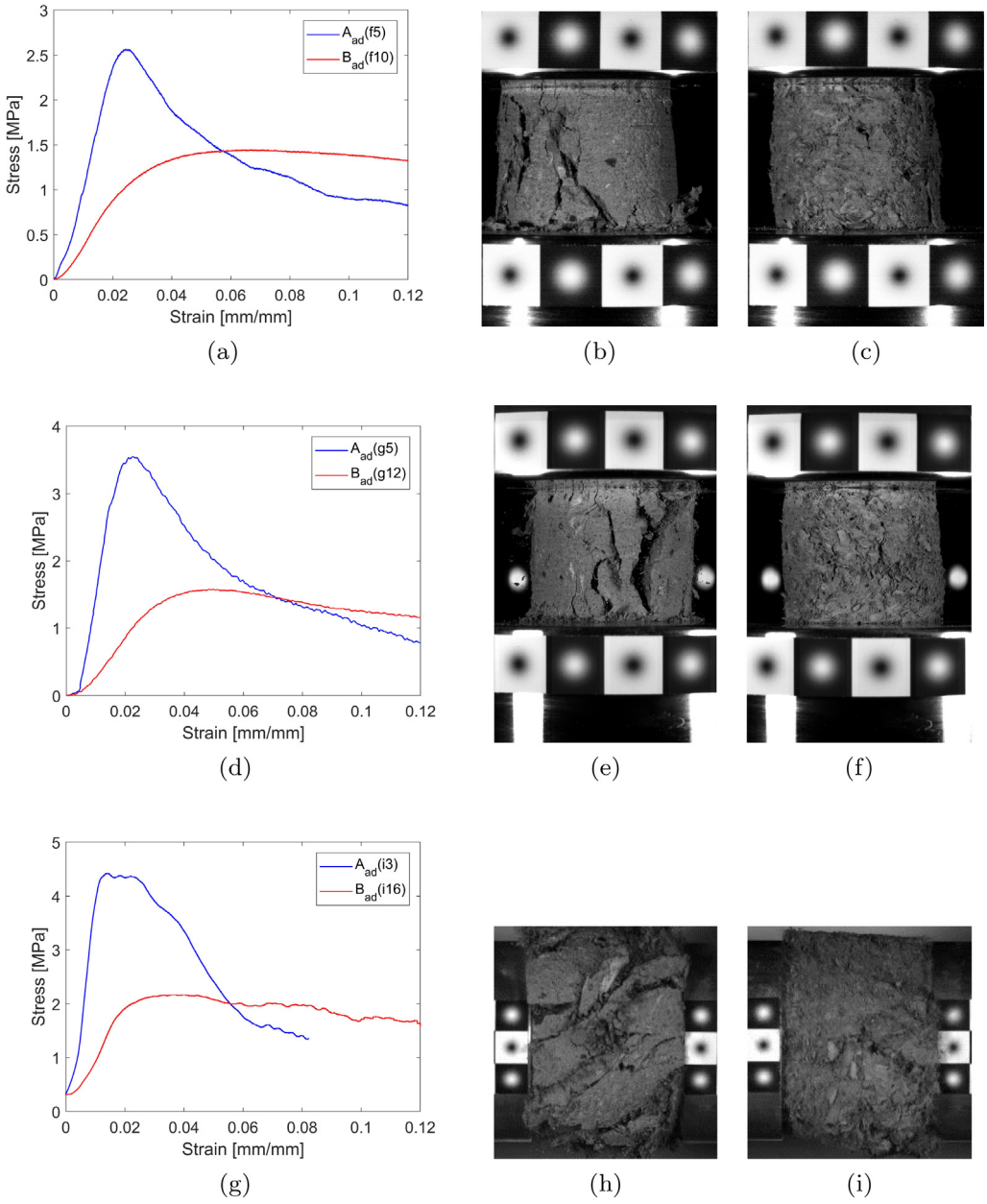

Fig. 6. Examples of stress strain plots and corresponding cracking patterns at 12% deformation for air dried Type A (left) and Type B (right) for static test (first row), intermediate strain rate test (second row) and split Hopkinson bar test (third row).

of the reference parameters in Eq. (2) (f_{bo} and $\dot{\epsilon}_s$) are adapted on tests on adobe. This is shown in Fig. 13, where the f_{bo} of the CEB formula is equal to 1.35 MPa, taken as the average of the compressive strength of 110 static tests collected from literature for traditional adobe in [20]. Other versions of the CEB formula are recently found in literature to address high performing steel fibre concrete (SFRC). Few tests found to address dynamic strength of concrete mixed with steel fibre proportions lower than 5% b.w. reveal lower sensitivity to rate with respect to plain concrete [40–42]. In [41], the CEB model was modified prolonging the yielding strain rate ($\dot{\epsilon}_s = 53\ s^{-1}$) and decreasing the dynamic increase factor beyond with approximately a factor 0.7. In Fig. 13 the resulting function for a high performing concrete of strength of 80 MPa is shown. The plot is closer to the lower experimental rate of enhancement showed by fibre reinforced adobe. Underestimation of experimental data of adobe is also encountered considering other bi-linear functions for concrete tested on different dataset. This is the case of the function proposed by Tedesco and Ross and described in Eq. (3) [10].

$$\begin{cases} DIF = 0.00965\dot{\epsilon} + 1.058 \ for\ \dot{\epsilon} \leqslant 63.1\ s^{-1} \\ DIF = 0.758\ \dot{\epsilon} - 0.289 \ for\ \dot{\epsilon} > 63.1\ s^{-1} \end{cases} \tag{3}$$

Aside from piecewise functions in standards, monotonically increasing equations with power or logarithmic shapes are used in literature to define rate dependent models for quasi brittle materials (Eqs. (4) and (5)):

$$DIF = \left(\frac{\dot{\epsilon}}{\dot{\epsilon}_s}\right)^{\alpha} \tag{4}$$

$$DIF = A_o + A_1 log\left(\frac{\dot{\epsilon}}{\dot{\epsilon}_s}\right) + A_2 log^2\left(\frac{\dot{\epsilon}}{\dot{\epsilon}_s}\right) + (\ldots) A_n log^n\left(\frac{\dot{\epsilon}}{\dot{\epsilon}_s}\right) \tag{5}$$

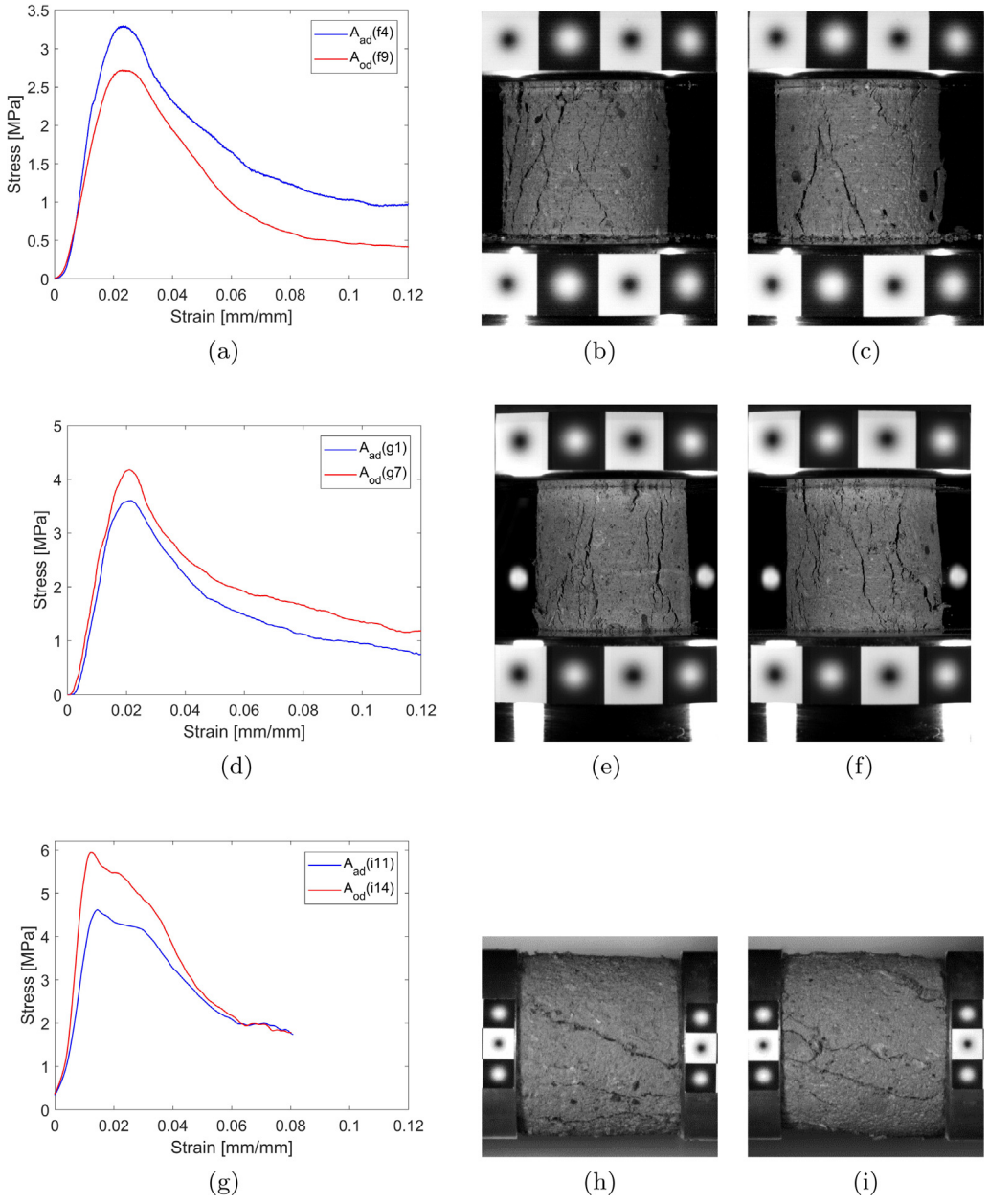

Fig. 7. Examples of stress strain plots and corresponding cracking patterns at 50% stress decay for air dried (b, e, h) and oven dried (c, f, i) Type A for static test (first row), intermediate strain rate test (second row) and split Hopkinson bar test (third row).

Table 2
Average values (and standard deviations) for the main material properties in compression at the three different strain rates for the two types and drying conditions. A_{ad} = Type A, air dried; A_{od} = Type A, oven dried; B_{ad} = Type B, air dried; B_{od} = Type B, oven dried.

Strain Rate	Parameter	Type			
		A_{ad}	A_{od}	B_{ad}	B_{od}
$\dot{\epsilon}_1$ (s^{-1})	f_b [MPa]	2.6(0.2)	3.3(0.1)	1.4(0.2)	1.6(0.1)
	E [MPa]	170(34)	267(29)	54(7)	65(11)
	ϵ_{f_b} [%]	2.4(0.3)	2.2(0.2)	5.7(0.6)	5.6(0.6)
	ϵ_u [%]	3.7(0.2)	3.5(0.1)	12.1(0.2)	12.9(0.3)
$\dot{\epsilon}_2$ (s^{-1})	f_b [MPa]	3.5(0.1)	4.2(0.1)	1.6(0.2)	1.8(0.1)
	E[MPa]	208(60)	306(59)	68(11)	71(10)
	ϵ_{f_b} [%]	2.5(0.4)	2.3(0.3)	5.2(0.3)	5.3(0.4)
	ϵ_u [%]	3.7(0.2)	3.4(0.2)	13.2(0.3)	13.3(0.1)
$\dot{\epsilon}_3$ (s^{-1})	f_b [MPa]	4.8(0.3)	5.6(0.5)	2.3(0.2)	2.6(0.3)
	E [MPa]	300(40.1)	401(50)	84(12)	92(10)
	ϵ_{f_b} [%]	1.8(0.1)	1.6(0.3)	4.5(0.4)	4.5(0.4)
	ϵ_u [%]	3.7(0.5)	3.5(0.5)	13.6(0.5)	13.1(0.6)

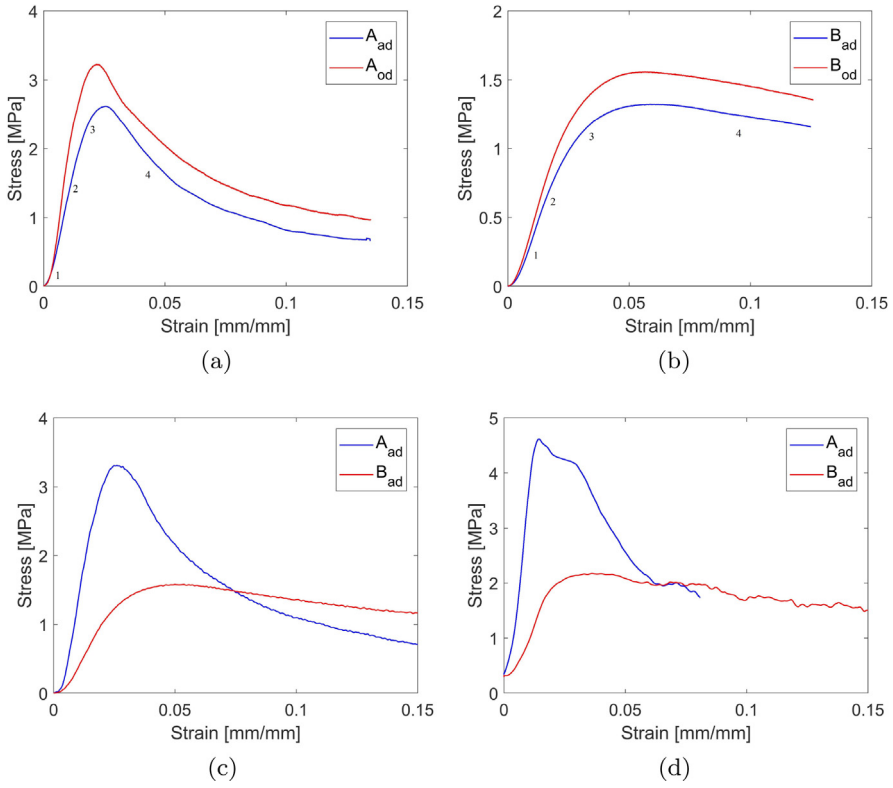

Fig. 8. Average normalized stress-strain plots for Type A and Type B in statics for both drying conditions (a, b) and in dynamics at intermediate strain rates (c) and split Hopkinson bar tests (d) for air dried condition.

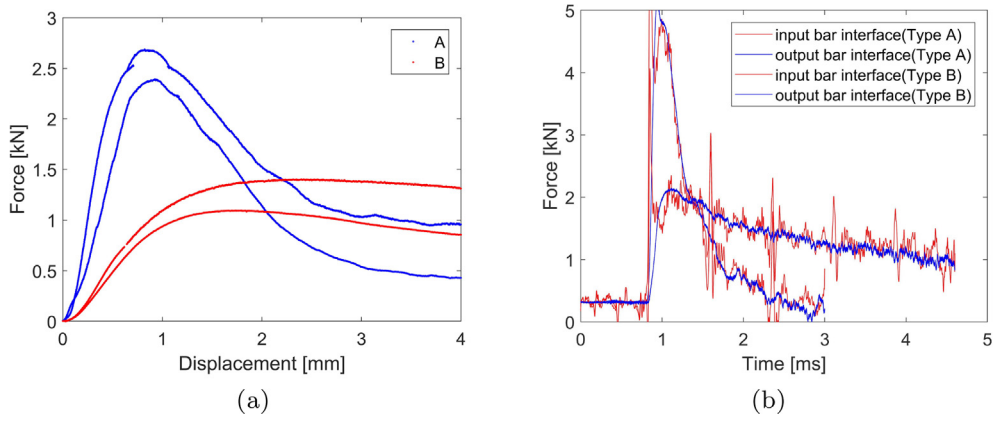

Fig. 9. Typical envelopes of the response curves (a) and specimen equilibrium check at interfaces between the transmitted and the input-reflected resultant wave during a split Hopkinson bar test (b) for air dried Type A and Type B.

where n defines the degree of the function and $A_0 - A_n$ and α are non dimensional parameters to be determined according to interpolation of extensive experimental dataset. Most formulations belong to the second class [43] (Eq. (5)) while the model proposed by Mihashi and Wittman in [44] belongs to the first approach based on a stochastic theory of fracture in conjunction with thermodynamics (where α is equal to $\frac{1}{1+\beta}$ with β a material parameter to be interpolated) [45].

Eqs. (4) and (5) can be used to interpolate the average strengths of adobe types at different strain rates. Interpolation was based on least square method on mean compressive strength for both types and water contents. Examples of interpolating functions (for Type A_{ad}) are shown in Fig. 13 for each equation. Best fit parameters and mean errors are reported for both types of functions and tested adobe in Table 3. The power function does not address satisfactorily experimental data on adobe. It tends to overestimate the dynamic strength at intermediate strain and to under-value the maximum dynamic strength above $\dot{\epsilon} = 100\ s^{-1}$. Best fit values are however slightly higher than the ones proposed originally ($\beta = 14$ for flexural strength) [44].

An overall better approximation is obtained using third order logarithmic functions. Best fit values are lower than the usual ones proposed for concrete materials and are contained in a narrow range for the two types at different drying conditions (Table 3) [5].

An integrative approach consists in using these rate dependent formulations to extend the validity of constitutive models developed in statics to the dynamic regime. In fact, for masonry materials the whole softening curve of response, besides the quantification of the value of strength, is important in case of nonlinear dynamic analyses [46]. This was the approach used by

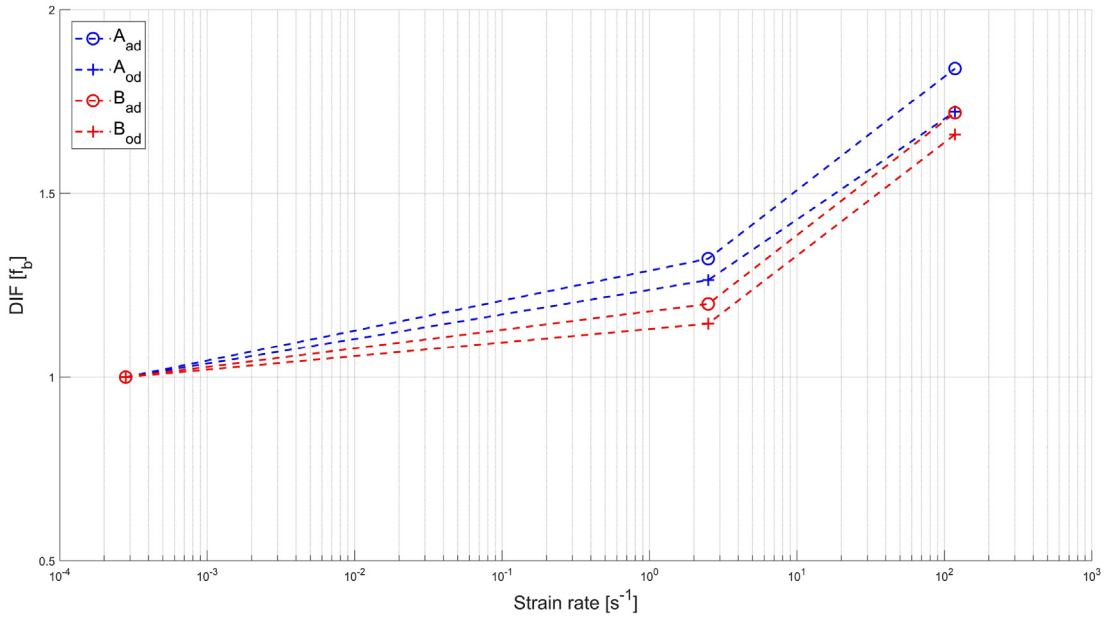

(a)

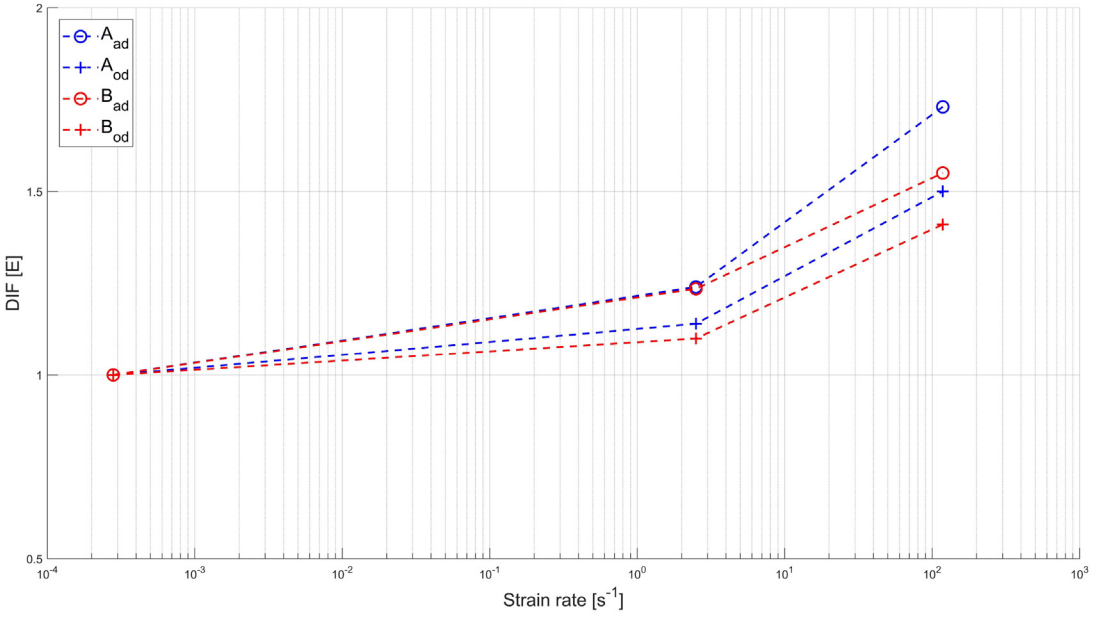

(b)

Fig. 10. Dynamic increase factor in strength (a) and elastic modulus (b) for both types and drying conditions.

Priestley et al. in [47], where analytical $\sigma - \epsilon$ curves developed for the constitutive assessment of concrete masonry in statics ($\dot{\epsilon} = 3\ 10^{-6}\ s^{-1}$) were adapted via a multiplying factor of 1.25 for both deformation and strength parameters of the model to simulate the mechanical response at $\dot{\epsilon} = 0.01\ s^{-1}$. A similar approach is attempted in this section. A constitutive model from literature is proposed for the static assessment of the tested adobe components [48–50]. In fact, statistical analyses confirm that models originally developed for concrete can be used to interpolate the curve of response of adobe [51,52]. In this case, the stress-strain equation in compression proposed by Popovics for normal concretes of given aggregates compositions [53] is used to address both the tested types and drying conditions of adobe in Section 2. The model is reported in Eq. (6) as:

$$\sigma = (E_o)\left(\frac{n}{n-1+\left(\frac{\epsilon E_o}{f_b}\right)^n}\right)\epsilon \tag{6}$$

where E_o is the ratio between the compressive strength and the corresponding strain while n is the only material parameter of the model, which in the original work of [54] varies between 2 and 4 for mortars and 1.5–5 for concrete according to porosity and internal matrix composition.

For each test of Section 2 in statics n was calibrated to match the curve of response at least until ultimate strain. The model fits well all experimental results of unfired bricks, independently from water and fibre inclusions in the mixture (Fig. 14(a,b)), with limited standard deviations for n associated to each type and drying

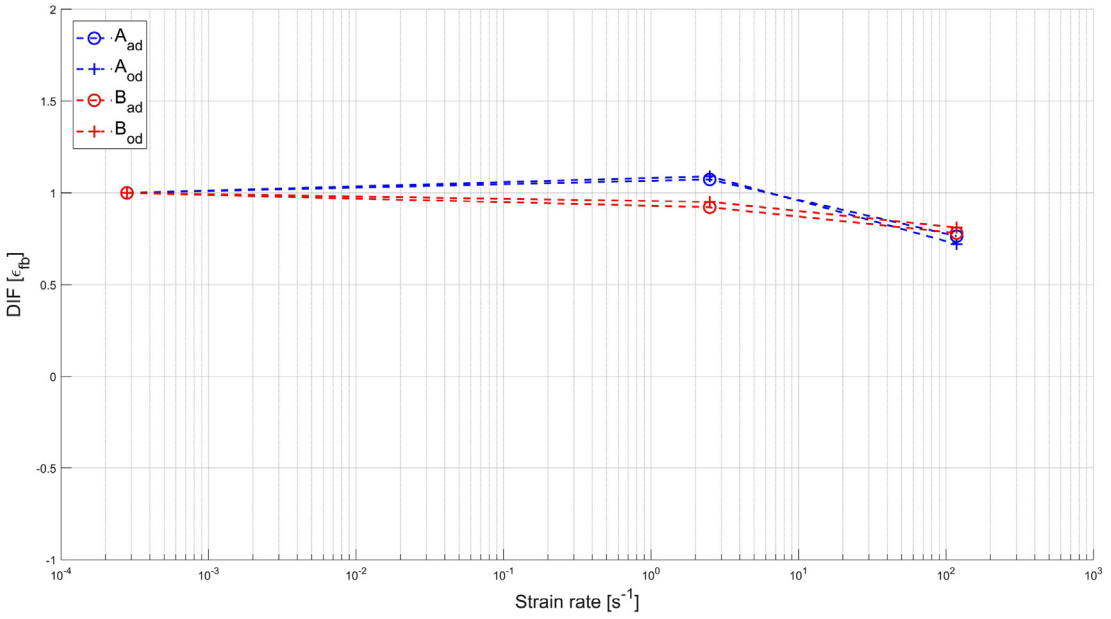

(a)

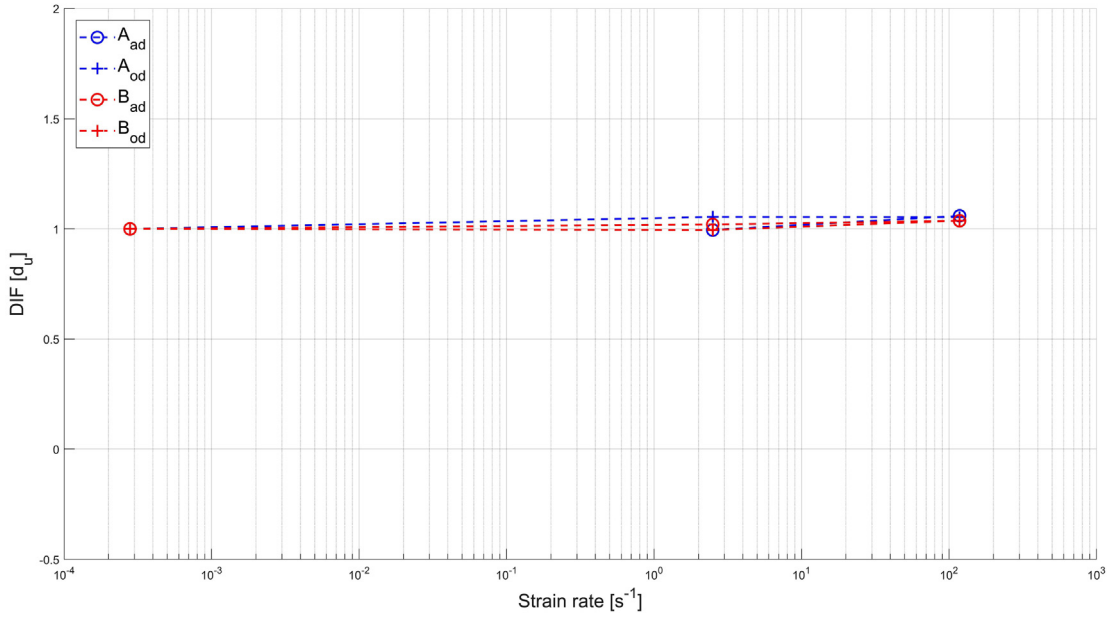

(b)

Fig. 11. Dynamic increase factor in critical strain (a) and ultimate displacement (b) for both types and drying conditions.

conditions. Mean best fit values for n are found to be almost double for fibre free air dried samples (3.1 ± 0.2) compared to fibre reinforced ones (1.7 ± 0.1). Values slightly differed if samples were oven dried both for Type A (3.0 ± 0.2) and Type B (1.7 ± 0.1). As in [53], statistical inference suggests that n is a property of the soil mixture quantitatively linked to the 18% of fibres added in the soil mixture. A value of 3 and 1.7 respectively for Type A and Type B is thus kept as a material constant for the constitutive assessment of adobe in dynamics. Similarly to [47] approach, Eq. (6) is thus modified in dynamics to:

$$\sigma = (kE_o)\left(\frac{n}{n-1+\left(\frac{\epsilon k E_o}{DIF\ f_b}\right)^n}\right)\epsilon \tag{7}$$

where DIF corresponds to the best fit functions calibrated for each type and drying conditions in Eq. (5) and k is a function on the dynamic strength enhancement statistically derived by interpolating all dynamic functions for each type, drying conditions and applied rate. As a result of multivariate analyses, a formulation for k is derived:

$$\frac{k}{DIF} \approx 1 + (3e^{-3}n - 3e^{-3})(1 + 0.03w)\dot{\epsilon} \tag{8}$$

where statistical inferences confirms higher sensitivity for higher water content (w) and minor organic content (n). Fig. 14(c–f) show the analytical-experimental comparisons between the constitutive model calibrated in statics integrated with rate

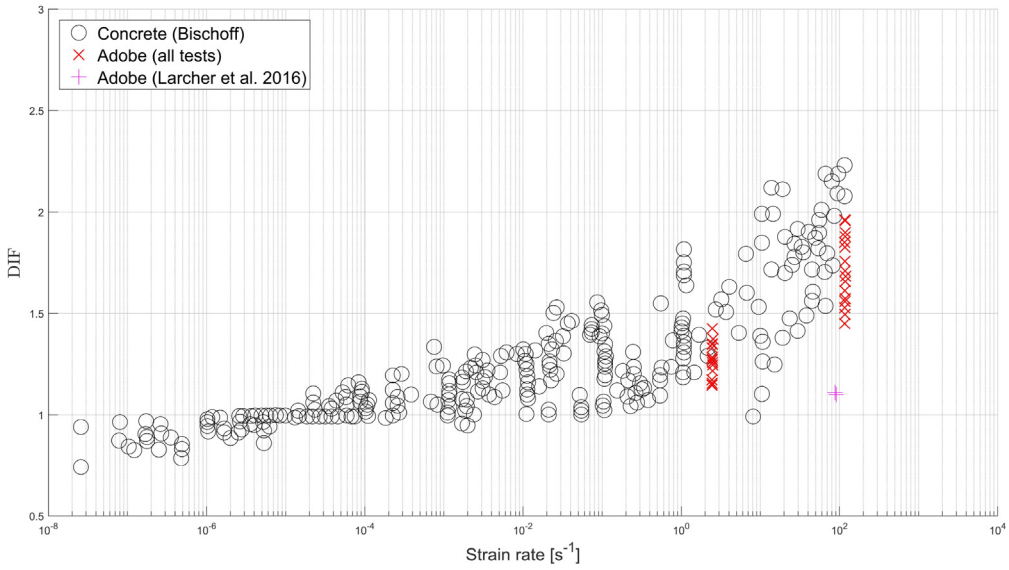

Fig. 12. Typical dynamic increase factors in compressive strength for concrete and test results for adobe.

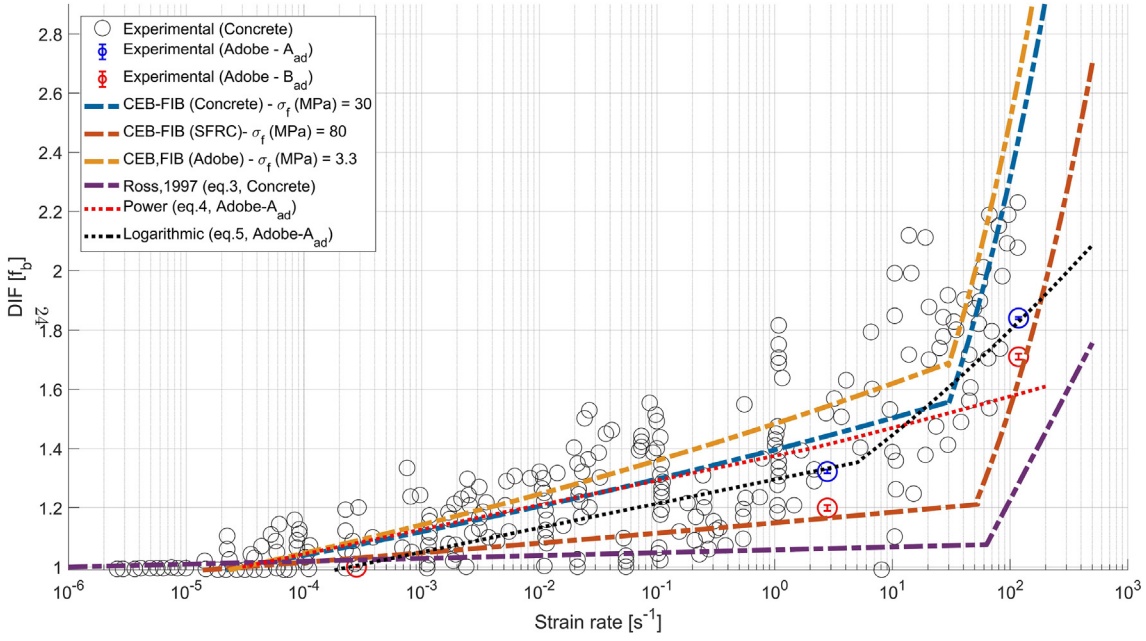

Fig. 13. Different DIF functions for the assessment of the dynamic compressive strength of adobe ($TypeA_{ad}$) at various strain rates.

Table 3
Best fit parameters (rounded to the first significant digit) for logarithmic and power functions and square roots errors

Type	Logarithmic					Power	
	A_o	A_1	A_2	A_3	err	β	err
A_{ad}	0.7	0.03	0.03	≃0.0	0.01	27	0.2
A_{od}	0.7	0.03	0.03	≃0.0	0.02	31	0.1
B_{ad}	0.5	0.02	0.03	≃0.0	0.02	34	0.1
B_{od}	0.5	0.02	0.03	≃0.0	0.02	36	0.2

dependent functions and the mean experimental curves for each type, drying conditions and strain rates. Considering the wide range of strain rates targeted and the natural scatter inherent tests on not engineered materials, the model well addresses the experimental data on adobe also in dynamics. This is particularly the case for Type B.

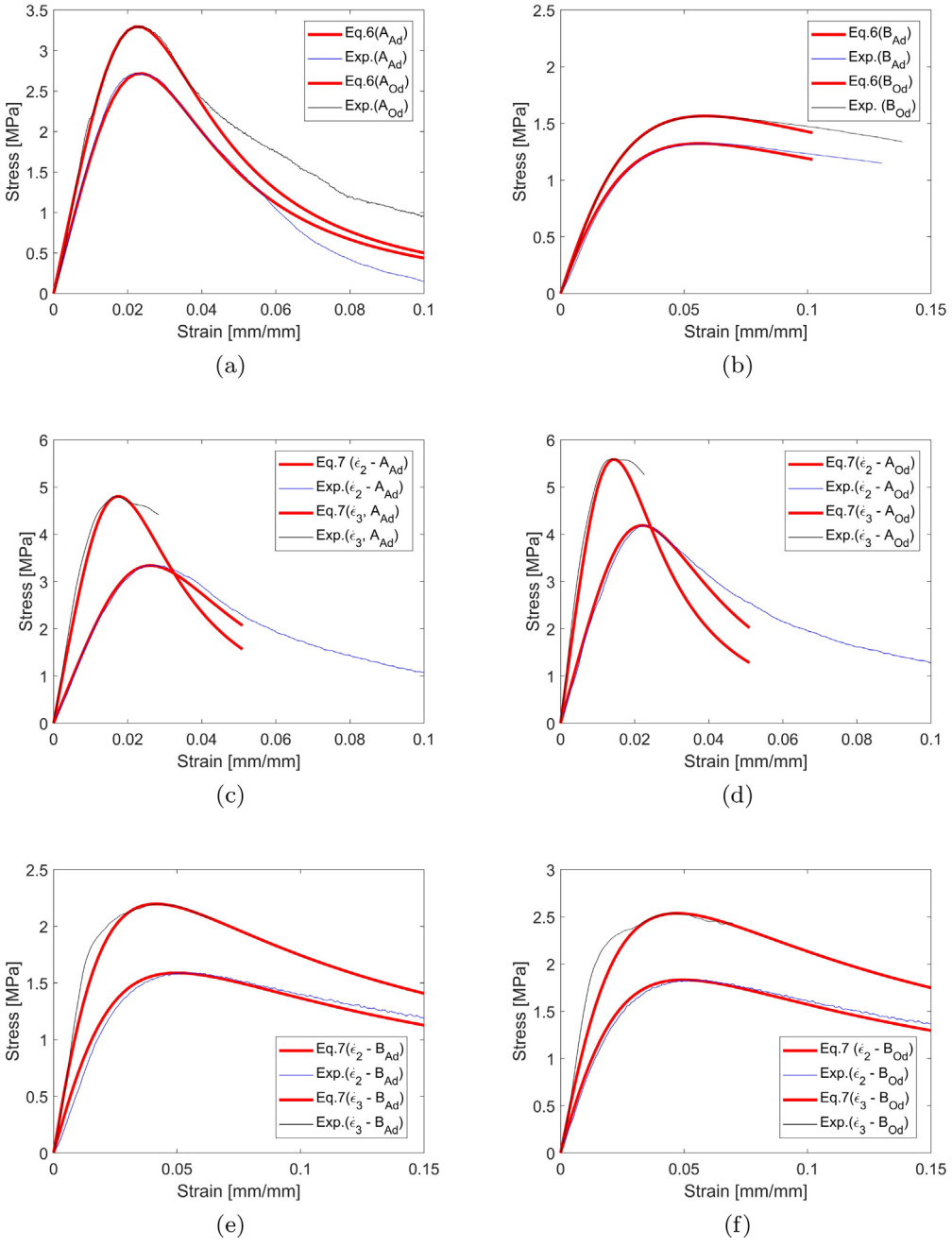

Fig. 14. Experimental-analytical comparison in statics for air dried and oven dried Type A (a) and Type B (b) and experimental analytical comparison in dynamics at both strain rates ($\dot{\epsilon_2}$ and $\dot{\epsilon_3}$) for air dried Type A and Type B (c, d) and oven dried (e, f).

4. Discussion: interpreting the role of fibers and water content in statics and dynamics

The experimental study has revealed that the mechanical performance of adobe is sensitive to the applied strain rate and its material resistance is enhanced when solicited by dynamic loadings. Analysis of data proves that macro-models developed for cementitious materials are suitable to simulate the mechanical response of adobe components [51] and the associated DIF parameters are within the same experimental ranges usually associated to modern geomaterials as concrete and mortar [5,55].

This section focuses on the meso-scale interpretation of the role of fibres and water content in adobe mixtures according to the observed patterns in Section 2,3. As cement and concrete, adobe is a quasi-brittle geomaterial which can be considered as macroscopically homogeneous at a certain length scale. However, the physical interpretation of the mechanisms which are activated inside the material of adobe when solicited by dynamic loadings can not be done without a detailed analysis of its mesostructure. Each component in adobe, including water and air pores, plays a role and interacts with the others in the mixture according to mineralogical properties and production processes determining the overall system strength. Its rigorous assessment is possible only using advanced experimental techniques [30]. These have been largely used to investigate the behaviour of modern building materials but they have been only rarely applied on adobe [56].

Furthermore, production processes in adobe are not standardized and quantity, materials and proportions of mixture components are often decided in the field according to local availability and different vernacular building traditions.

However, water and fibre content were the isolated variables of this experimental study and analysed for a wide range of loading conditions from statics to high velocity impacts. Thus, the resulting information constitutes a solid qualitative as well as quantitative dataset which allows to propose interpretations on the effect of fibres and water content in the meso-structure on the macro-properties of adobe at different rates. For both factors, interpretation starts from the analysis of the dynamic behaviour exhibited by adobe and they are verified with respect to the trends observed in statics. The resulting theory for adobe resorts to principles of fracture mechanics and of geotechnics and soil investigations, which are actually commonly adopted also to interpret the micro-behaviour in modern geo-based building materials.

4.1. Water in adobe mixtures: the role of chemical bonds

The higher sensitivity in strength to high strain rates exhibited by samples containing interstitial water is explained at a meso scale by "*Stefan adhesion*" [57]. According to this principle of viscosity, a layer of water between two parallel plates separated by a certain distance exerts a normal force which is proportional to the velocity with which the plates are approximated or separated [58]. This inter-capillary phenomenon is supposed to happen between the surfaces of soil particles of adobe solicited by high velocities of deformation (Fig. 15) [59].

The Stefan effect has been used to interpret the dependence of moisture content on dynamic performances which have been observed also for concrete [7,60,61]. Tests on concrete samples in tension revealed that rate sensitivity in tensile strength can almost double when saturated with respect to normal cured concrete [61]. The lower sensitivity shown by the tested adobe is explained by the low water content in samples air cured under sun for 28 days and by the possible effect of high water reactivity inherent in clay toward water [62].

Inter-particle chemical bonds explain also the higher static performance associated to fully dried adobe tested in the study. Interstitial water weakens the bonds between binder particles in the mixture. Its evaporation allows the formation of stronger chemical binding which ensure a denser inter-particle arrangement [63]. This is consistent with the Lambe's model for compacted soils: on a dry state, the distance between two clay platelets is small enough for the Van der Waal forces to dominate, inducing clay flocculation and making up the structure [64,62].

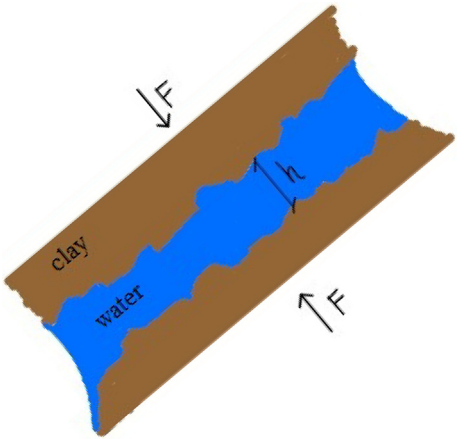

Fig. 15. Schematic picture of Stefan effect between two clay floccules (Source: authors).

Also for concrete materials, higher strength is observed in literature for baked cement pastes with respect to normal cured concrete [41,30]. Fibre free baked adobe reveals values for static strength which are comparable with some building materials commonly used for masonry constructions. Table 4 compares the mean strength of baked adobe with respect to values associated to other modern building materials used for masonry [65]. Comparison reveals that oven dried strength of fibre free adobe is close to lightweight aerated concrete.

The drying process does not significantly influence the deformation capacity of adobe in statics and dynamics [20]. This is related to the cracking process of the material, which is associated to the role of fibres in the matrix [66]. This is discussed in the following paragraph. Areas of the matrix inherent fibres are considered as fully dried after 28 days of curing. This is consistent with the observation of similar water content for the two types in Par. 2.1 despite different fibre amount: fibres and surrounding areas are fully dried while water is retained in clay and at interstitial level of the matrix.

4.2. Fibres in adobe mixtures: the role of heterogeneity

The lower sensitivity of strength to high strain rates exhibited for adobe samples containing fibres is interpreted by linking principles of fracture mechanics to hypotheses on the specific heterogeneity level of fibre enriched mixtures of adobe. Actually, as showed in Section 3, also the few multi-strain rate experimental tests available in literature on fibre reinforced concrete reveal a lower DIF compared to plain concrete. This was also explained for concrete as a result of a higher homogeneity and lower porosity levels provided by steel fibres at a meso-scale [41,40]. This is consistent with the positive effects of fibres on the toughness and strength of the material in statics [67]. In fact, fibres in concrete have been lately added in the mixtures to enhance the mechanical performance of the material through the employment of the specific mechanical properties of both elements and including their proper interaction. Instead adding fibres represents an ancient practice for adobe, originally meant to reduce shrinkage cracks inherent to air drying processes of bricks mixtures during production processes.

Interpretation provided in this study on the role of fibres on the mechanical performance of adobe both in dynamics and statics requires to mention a few fracture mechanics principles.

For a generic quasi brittle material tested in dynamics, the enhancement of strength performance can be explained considering a change of fracture planes at a meso-scale with respect to statics [7]. In statics, given a limited set of flaws inside the material, the most critically sized and oriented ones undergo crack initiation and propagation. As these microcracks approach the vicinity of other propagating ones, they may interact and coalesce into a macro crack which leads to loss of structural integrity and failure at a macro-scale [68,69]. In fact, if propagating flaws encounter stiffer areas, they have the time to deviate around them bridging into macro-cracks and the fracture and stress path with minimum energy demand is defined. Instead in dynamics, loadings characterized by short time duration and high supply rates induce a forced crack development inside the material also through its stiffer areas, while stress intensity is reduced by the coalescence of other similar micro-cracks nearby the loaded areas [70]. As a result, more diffuse patterns of short and straight cracks initiated at multiple weak spots are often observed in quasi brittle materials such as concrete, corresponding to higher values for compressive strength and strain at peak [7,26]. Also in adobe a strength enhancement is displayed at high strain rates, which is lower than the typical ranges

Table 4
Comparison of compressive strength of different masonry materials (HC: hollowed clay; CS: calcium silicate; LAC: lightweight concrete; AAC: autoclaved aerated concrete; AD: oven dried fiber free adobe) using the database for masonry in [65].

Parameter	Material				
	HC	CS	LAC	AAC	AD
Strength [MPa]	16.9	26.1	14	3.8	3.3

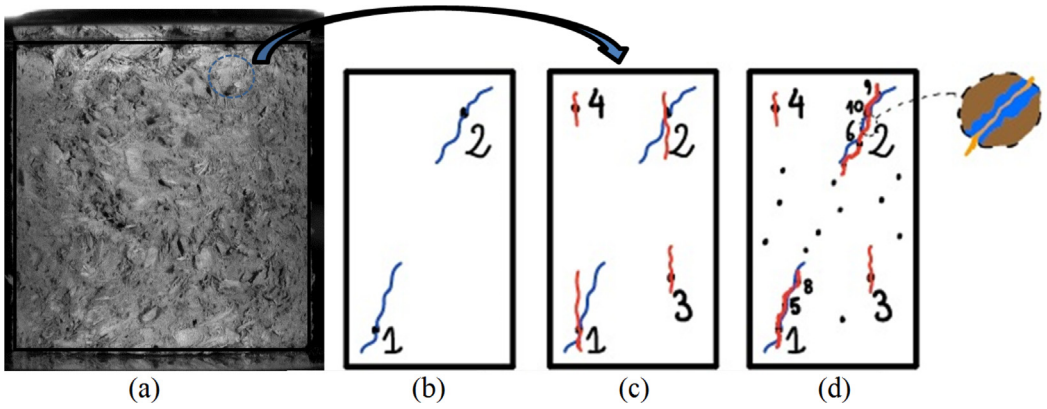

Fig. 16. Specimen (a) and schematic meso-scale representation of micro-flaws numbered in descending order of entity and crack paths, in blue lines for statics (b) and in red in dynamics for low (c) and high (d) number and density of flow distribution, with zoom on possible clay floccules separated by fibers.

associated to concrete. Cracking patterns in dynamics of the tested adobe clearly show parallel crack orientations to the loading direction only at the first stages of deformation in dynamics. This is especially the case for fibre enriched mixtures, which experience the lowest rate of increment in the performance and whose failure pattern in dynamics tends to follow the static ones with negligible influence of rate on deformation capacity. The theory of fracture mechanics links with the experimental evidence for adobe given that the rate of enhancement of the dynamic material properties depends on the spatial distributions of the micro-flaws inside the material, that is by the level of uniformity of a mixture. If the number of micro-flaws increases, the probability of interaction increases also in case of dynamic loadings [71]. It means that if density of initial flaws distribution is sufficiently high, the effect of loading rates on the crack bridging processes is limited and a stress path with energy demand close to statics can be developed also in the dynamic regime (Fig. 16). This interpretation can explain the lower DIF of adobe with respect to concrete and the lower DIF of fibre enriched mixtures with respect to fibre free ones. In fact, for industrialized cementitious materials, selection and production processes are highly standardized in order to ensure prescribed levels of uniformity to the mixture and resulting material performance. For adobe, appropriate material standards and related quality controls do not exist yet. Moreover, traditional adobe is not pressed during curing, potentially increasing the number of voids in the mixture. Therefore, the level of heterogeneity of traditional adobe is higher than the one associated to modern building materials. This is especially the case for mixtures containing organic content.

The interpretation of the role of fibres in adobe in dynamics is consistent with the experimental trends observed in statics. In fact, low levels of strength and stiffness associated to the tested adobe including fibres are commonly observed also in literature [72,20]. In this setting, fibres constitute weak interfaces of the soil matrix of adobe in statics [52]. Their inclusions in soil mixtures potentially determine extensive areas of de-adherence between the adopted soil matrix and natural organic materials, which enhance porosity in the mixture and exasperates the material heterogeneity [32]. Void distribution and porosity is in fact found to weaken the strength also in mortar used in modern masonry [73]. However, in rare cases, fibres are found to enhance macro properties in strength [74]. The success of fibre inclusion on the strength is indeed determined by the bonding between the different micro-elements which determines the meso structure of the mixture; that is by soil mineralogical family, elements proportions and organic materials, contents, sizes and shapes [52]. To a minor extent, this also counts for modern building materials. In steel reinforced concrete for instance, the level of bonding in the matrix is found to be dependent on the percentage of steel reinforcement [75].

The major contribution associated to the presence of fibres in the mixture on the mechanical performance of adobe is related to the material ductility. This is a common trend observed for the material of adobe in literature and this is considered the "reinforcing" effect on adobe [72] [76]. Its role is visible from early stages of deformation up to the softening phase of the material response and it is due to the stress-transfer occurring at meso-scale in the mixture. Presence of fibres determines higher heterogeneity to the mixture and larger number and areas of flaws, that causes a more pronounced non linear slope also in the pre-peak curve of response. However, the bridging effect of the fibres allow stresses to be transferred through cracks, limiting their entity and holding together the vital cores of the soil particles which are separated by fibres in the post peak region [77,78]. A similar role is attributed to fibre inclusion in concrete (SFRC), with fibres disperse in the matrix capable of holding together the matrix while reducing the overall lateral expansion of specimens [41,42].

Fibres are also confirmed to boost the physical properties of the mixture, decreasing the weight of the brick [79].

5. Conclusions

An experimental campaign was performed on specimens of adobe, a masonry made of unsaturated soil bricks and mud mortar. Two types of bricks were tested. They had the same mineralogical composition but they differed in the presence of organic content. For both, half of the samples were fully dried in the oven. Samples

were subjected to compressive loadings at three different strain rates corresponding to static, intermediate and high rate loading conditions. A substantial, high-quality set of experimental data has been produced. Data have been elaborated and some constitutive models originally developed for modern geomaterials have been reviewed and proposed for modelling the adobe strain rate sensitivity of strength in this study. In fact tests revealed that the material properties in strength are enhanced by the rate of loadings while a minor influence was encountered in the deformation performance. Strength rate increases more in fully air-dried adobe and in mixtures not containing fibres. This is interpreted as that water induces a viscous inter-capillary phenomenon which strengthens inter-particles bonds in the matrix proportionally to the rate of loading. Adding fibres in the mixture enhances the heterogeneity of material for adobe and fibres weaken inter-particle bonds in the matrix causing the presence of weak regions at a meso-scale.

It has also been shown that the macro-properties of adobe, including dynamic increase factors and softening curves, can be addressed using numerical models developed for concrete-based materials. However, many of these numerical models used in engineering are mainly based on assumptions of material homogeneity. This is an accepted approximation for modern building materials which are heterogeneous at a meso-scale but whose mixture selection and production processes are standardized to ensure prescribed levels of homogeneity at a given length scale. As explained above, this assumption can not be a priori transferred to the traditional adobe produced in the field. Adobe is still a site dependent material and the selection of the mineralogical and geometrical properties of the elements involved in the mixture is not standardized according to optimization requirements but rather chosen for opportunity reasons. In absence of manufacturing regulations and production chain control, high fibre fractions can cause serious material inhomogeneity and void increase in certain soil mixtures of adobe. Proper material selection and production procedures with resulting optimum product quality is essential to ensure a safe use to a sustainable material in current society.

Declaration of Competing Interest

The authors declare that they have no known competing financial interests or personal relationships that could have appeared to influence the work reported in this paper.

References

[1] https://ec.europa.eu/jrc/en/research/commission-priorities (2018).
[2] T. Li Piani, Operative Guidelines for Protection of Places of Worship: A New Approach Toward Security Design of Sensitive Buildings, Institute for Advanced Strategic and Political Studies, Milan, 2017. ISBN: 97888940373-2-6.
[3] J. Coaffee, P. O'Hare, M. Hawkesworth, The visibility of (in)security: the aesthetics of planning urban defences against terrorism, Secur. Dialogue 40 (4–5) (2009) 489–511, https://doi.org/10.1177/0967010609343299.
[4] T. Li Piani, Structural design and the social function of space as vulnerability factor and solution to the progression of the terrorist threat in urban environments (italian), Secur. Terror. Soc. (STS) 8 (2) (2018) 7–17.
[5] D. Grote, S. Park, M. Zhou, Dynamic behavior of concrete at high strain rates and pressures: I. Experimental characterization, Int. J. Impact Eng. 25 (9) (2001) 869–886, https://doi.org/10.1016/S0734-743X(01)00020-3.
[6] P. Forquin, Brittle materials at high-loading rates: an open area of research, Philos. Trans. R. Soc. A 375 (2085) (2017) 20160436, https://doi.org/10.1098/rsta.2016.0436.
[7] R. Pedersen, Computational Modelling of Dynamic Failure of Cementious Materials (Ph.D. thesis), Delft University of Technology, Tu Delft, 2010.
[8] J. Baylot, B. Bullock, T. Slawson, S. Woodson, Blast response of lightly attached concrete masonry units walls, J. Struct. Eng. 131 (8) (2005) 1186–1193.
[9] H. Hao, B. Tarasov, Experimental study of dynamic material properties of clay brick and mortar at different strain rates, Aust. J. Struct. Eng. 8 (2) (2008) 117. URL:http://search.informit.com.au/documentSummary;dn=137784543477420;res=IELENG.
[10] Q.M. Li, Y.B. Lu, H. Meng, Further investigation on the dynamic compressive strength enhancement of concrete-like materials based on split Hopkinson pressure bar tests. Part II: numerical simulations, Int. J. Impact Eng. 36 (12) (2009) 1335–1345, https://doi.org/10.1016/j.ijimpeng.2009.04.010.
[11] P. Bischoff, S. Perry, Impact behavior of plain concrete loaded in uniaxial compression, J. Eng. Mech. 121 (June) (1995) 685–693, https://doi.org/10.1061/(ASCE)0733-9399(1995) 121:6(685).
[12] X. Wei, H. Hao, Numerical derivation of homogenized dynamic masonry material properties with strain rate effects, Int. J. Impact Eng. 36 (3) (2009) 522–536, https://doi.org/10.1016/j.ijimpeng.2008.02.005.
[13] J.M. Pereira, A. Dias, P.B. Lourenço, Dynamic properties of clay brick at different strain rates, Proc. of the 12th, Can. Masonry Symp. 1300 (1990) (2013).
[14] M. Larcher, M. Peroni, G. Solomos, N. Gebbeken, P. Bieber, J. Wandelt, N.T. Tran, Dynamic Increase Factor of Masonry Materials: Experimental Investigations, 2013.
[15] D. Silveira et al., Mechanical properties of adobe bricks in ancient constructions, Constr. Build. Mater. 28 (1) (2012) 36–44, https://doi.org/10.1016/j.conbuildmat.2011.08.046.
[16] P.W. Brown, J.R. Clifton, The properties of adobe, in: International Institute for Conservation of Historic and Artistic Works, Taylor & Francis, Ltd, 1978, pp. 139–146. 23.
[17] B. Briseghella, V. Colasanti, L. Fenu, C. Nuti, E. Spacone, H. Varum, Seismic analysis by macroelements of fujian hakka tulous, chinese circular earth constructions listed in the UNESCO world heritage list, Int. J. Archit. Heritage (2019) 1–16, https://doi.org/10.1080/15583058.2019.1618973.
[18] Adobe masonry in current society: material performance under extreme events (https://www.youtube.com/watch?v=2mxwoS9vFlw) (2018).
[19] D. Silveira, H. Varum, A. Costa, Influence of the testing procedures in the mechanical characterization of adobe bricks, Constr. Build. Mater. 40 (2013) 719–728, https://doi.org/10.1016/j.conbuildmat.2012.11.058.
[20] T. Li Piani, D. Krabbenborg, J. Weerheijm, L. Koene, L.J. Sluys, The mechanical performance of traditional adobe masonry components: an experimental-analytical characterization of soil bricks and mud mortar, J. Green Build. 13 (3) (2018) 17–44.
[21] A.A. Hammond, Prolonging the life of earth buildings in the tropics, Build. Res. Pract. 1 (3) (1973) 154–163, https://doi.org/10.1080/09613217308550234.
[22] F. Pacheco-Torgal, S. Jalali, Earth construction: lessons from the past for future eco-efficient construction, Constr. Build. Mater. 29 (2012) 512–519, https://doi.org/10.1016/j.conbuildmat.2011.10.054.
[23] E.J.d.P. Hansen, K. Kielsgaard Hansen, Unfired clay bricks – moisture properties and compressive strength, in: A. Gustavsen, J.V. Thue (Eds.), Proceedings of the 6th Symposium on Building Physics in the Nordic Countries, vol. 2, Norwegian University of Science and Technology, 2002, pp. 453–460.
[24] R. Yu, P. Spiesz, H.J. Brouwers, Static properties and impact resistance of a green ultra-high performance hybrid fibre reinforced concrete (UHPHFRC): experiments and modeling, Constr. Build. Mater. 68 (2014) 158–171, https://doi.org/10.1016/j.conbuildmat.2014.06.033.
[25] S.R. Ferreira, M. Pepe, E. Martinelli, F. de Andrade Silva, R.D. Toledo Filho, Influence of natural fibers characteristics on the interface mechanics with cement based matrices, Compos. Part B 140 (September 2017) (2018) 183–196, https://doi.org/10.1016/j.compositesb.2017.12.016.
[26] P.H. Bischoff, S.H. Perry, Compressive behaviour of concrete at high strain rates, Mater. Struct. 24 (6) (1991) 425–450, https://doi.org/10.1007/BF02472016.
[27] EN 772-1:2000, Methods of test of masonry units: determination of compressive strength.
[28] BS 1377-2: 1990, Methods of test for soils for civil engineering purposes, Classification tests.
[29] NT Build 333: Bricks and masonry blocks: Moisture content (1988). .
[30] I. Vegt, Concrete in Dynamic Tension: The Fracture Process (PhD thesis), TU Delft, 2016, https://doi.org/10.4233/uuid.
[31] M. Peroni, G. Solomos, N. Babcsan, Development of a Hopkinson bar apparatus for testing soft materials: application to a closed-cell aluminum foam, Materials 9 (1) (2016), https://doi.org/10.3390/ma9010027.
[32] R. Illampas, D.C. Charmpis, I. Ioannou, Dynamic finite element analysis of earth masonry structures based on experimental material data, Conf. Comput. Methods Struct. Dyn. Earthquake Eng. (May) (2011) 26–28.
[33] E. Cosenza, G. Maddaloni, G. Magliulo, M. Pecce, R. Ramasco, Seismic Design of Concrete Structures (Italian), Iuss Press, Pavia, 2007.
[34] S. Mishra, H. Meena, V. Parashar, A. Khetwal, T. Chakraborty, V. Matsagar, P. Chandel, M. Singh, High strain rate response of rocks under dynamic loading using split hopkinson pressure bar, Geotech. Geol. Eng. 36 (1) (2017) 531–549, https://doi.org/10.1007/s10706-017-0345-2. URL:http://link.springer.com/10.1007/s10706-017-0345-2.
[35] T. Li Piani, J. Weerheijm, M. Peroni, L. Koene, G. Solomos, L.J. Sluys, Dynamic characterization of adobe in compression: the effect of fibre fraction in soil matrix, in: FraMCoS-X: Fracture Mechanics of Concrete and Concrete Structures, Bayonne (France), 2019.
[36] N. Gebbeken, T. Linse, T. Araújo, Masonry under dynamic actions: experimental investigations, material modeling and numerical simulations, Adv. Prot. Struct. Res. 2012 (October 2015) 131–161, https://doi.org/10.1201/b12768-6.
[37] Z. Liang Wang, Y. Chi Li, R.F. Shen, J.G. Wang, Numerical study on craters and penetration of concrete slab by ogive-nose steel projectile, Comput. Geotech. 34 (1) (2007) 1–9, https://doi.org/10.1016/j.compgeo.2006.09.001.
[38] CEB (Comite Euro-International du Beton): CEB-FIP Model Code (1990).
[39] X.Q. Zhou, H. Hao, Modelling of compressive behaviour of concrete-like materials at high strain rate, Int. J. Solids Struct. 45 (17) (2008) 4648–4661, https://doi.org/10.1016/j.ijsolstr.2008.04.002.

[40] L. Yang, X. Lin, R.J. Gravina, Evaluation of dynamic increase factor models for steel fibre reinforced concrete, Constr. Build. Mater. 190 (2018) 632–644, https://doi.org/10.1016/j.conbuildmat.2018.09.085.
[41] S. Wang, M.-H. Zhang, S.T. Quek, Effect of high strain rate loading on compressive behaviour of fibre-reinforced high-strength concrete, Magn. Concr. Res. 63 (11) (2011) 813–827, https://doi.org/10.1680/macr.2011.63.11.813.
[42] Z. Wu, C. Shi, W. He, D. Wang, Static and dynamic compressive properties of ultra-high performance concrete (UHPC) with hybrid steel fiber reinforcements, Cem. Concr. Compos. 79 (2017) 148–157, https://doi.org/10.1016/j.cemconcomp.2017.02.010.
[43] X. Chen, S. Wu, J. Zhou, Experimental and modeling study of dynamic mechanical properties of cement paste, mortar and concrete, Constr. Build. Mater. 47 (2013) 419–430, https://doi.org/10.1016/j.conbuildmat.2013.05.063.
[44] H. Mihashi, F.H. Wittmann, Stochastic approach to study the influence of rate of loading on strength of concrete, Heron 25 (3) (1980).
[45] K.S.H.O.K. Jitsu, K. Shirai, C. Ito, Effects of strain rate on concrete strength subjected to impact load-Dynamic compressive strength test by Split Hopkinson Pressure Bar method, Trans. Built Environ. 32 (1998) 1–3.
[46] H.B. Kaushik, D.C. Rai, S.K. Jain, Stress-strain characteristics of clay brick masonry under uniaxial compression, J. Mater. Civ. Eng. 19 (9) (2007) 728–739, https://doi.org/10.1061/(ASCE)0899-1561(2007) 19:9(728). URL:http://www.iitk.ac.in/nicee/RP/2007_Masonry_Properties_ASCE.pdf.
[47] B. Scott, R. Park, M. Priestley, Stress strain behaviour of concrete confined by overlapping hoops at low and high strain rates, ACI J. 79 (1) (1982) 13–27.
[48] T. Li Piani, J. Weerheijm, L. Koene, L.J. Sluys, Modelling the mechanical response of adobe components under uniaxial loading, Key Eng. Mater. 774 (2018) 650–657.
[49] D.C. Kent, R. Park, Flexural members with confined concrete, J. Struct. Div. ASCE 97 (1990) (1971).
[50] R. Illampas, I. Ioannou, D.C. Charmpis, Adobe bricks under compression: experimental investigation and derivation of stress – strain equation, Constr. Build. Mater. 53 (2014) 83–90, https://doi.org/10.1016/j.conbuildmat.2013.11.103.
[51] T. Li Piani, J. Weerheijm, L. Koene, L. Sluys, The Adobe delta damage model: a locally regularized rate-dependent model for the static assessment of soil masonry bricks and mortar, Eng. Fract. Mech. 206 (2019) 114–130, https://doi.org/10.1016/j.engfracmech.2018.11.026.
[52] T. Li Piani, J. Weerheijm, L.J. Sluys, Ballistic model for the prediction of penetration depth and residual velocity in adobe: a new interpretation of the ballistic resistance of earthen masonry, Defence Technol. 14 (5) (2018) 4–8, https://doi.org/10.1016/j.dt.2018.07.017.
[53] S. Popovics, A review of stress strain relationships for concrete, Am. Concr. Inst. J. 67 (3) (1970) 243–248.
[54] A. Popovics, numerical approach to the complete stress strain curve of concrete, Cem. Concr. Res. 3 (1973) 583–599.
[55] J.W. Tedesco, J.C. Powell, C.A. Ross, M.L. Hughes, A strain-rate-dependent concrete material model for ADINA, Comput. Struct. 64 (5–6) (1997) 1053–1067, https://doi.org/10.1016/S0045-7949(97)00018-7.
[56] Y. Millogo, M. Hajjaji, R. Ouedraogo, Microstructure and physical properties of lime-clayey adobe bricks, Constr. Build. Mater. 22 (2008).
[57] J. Stefan, Versuche über die scheinbare adhäsion, Sitzungs- berichte der Kaiserlichen Akademie der Wissenschaften, Mathematisch-Naturwissenschaftliche Classe 1 (1874) 713–735.
[58] P. Rossi, A physical phenomenon which can explain the mechanical behaviour of concrete under high strain rates, Mater. Struct. 24 (6) (1991) 422–424, https://doi.org/10.1007/BF02472015.
[59] S. Zeng, X. Ren, J. Li, Triaxial behavior of concrete subjected to dynamic compression, J. Struct. Eng. 139 (9) (2013) 1582–1592, https://doi.org/10.1061/(ASCE)ST.1943-541X.0000686. URLhttp://ascelibrary.org/doi/10.1061/%28ASCE%29ST.1943-541X.0000686.
[60] J. Cao, D.D. Chung, Effect of strain rate on cement mortar under compression, studied by electrical resistivity measurement, Cem. Concr. Res. 32 (5) (2002) 817–819, https://doi.org/10.1016/S0008-8846(01)00753-0.
[61] E. Cadoni, K. Labibes, C. Albertini, M. Berra, M. Giangrasso, Strain-rate effect on the tensile behaviour of concrete at different relative humidity levels, Mater. Struct. 34 (February) (2001) 21–26, https://doi.org/10.1007/BF02482196.
[62] P. Delage, M. Audiguier, Y.-J. Cui, M. Howat, Microstructure of a compacted silt, Can. Geotech. 33 (1996) 150–158.
[63] J.A. Calabria, W.L. Vasconcelos, A.R. Boccaccini, Microstructure and chemical degradation of adobe and clay bricks, Ceram. Int. 35 (2) (2009) 665–671, https://doi.org/10.1016/j.ceramint.2008.01.026.
[64] T. Lambe, The structure of compacted clay, J. Soil Mech. Found. Div. 84 (1958) 1–34.
[65] P. Morandi, L. Albanesi, F. Graziotti, T. Li Piani, A. Penna, G. Magenes, Constr. Build. Mater. 190 (2018) 593–611, https://doi.org/10.1016/j.conbuildmat.2018.09.070.
[66] F. Aymerich, L. Fenu, P. Meloni, Effect of reinforcing wool fibres on fracture and energy absorption properties of an earthen material, Constr. Build. Mater. 27 (1) (2012) 66–72, https://doi.org/10.1016/j.conbuildmat.2011.08.008.
[67] H. Singh, Steel Fiber Reinforced Concrete: Behavior, Modelling and Design – Chapter 2: Material Models, vol. 25, 2017.https://doi.org/10.1617/s11527-010-9596-6. URL:http://www.jsce.or.jp/committee/concrete/e/newsletter/newsletter05/JSCE-VIFCEA Joint Seminar Papers.htm%0Ahttp://pubsindex.trb.org/view.aspx?id=25485.
[68] M. Jirasek, Z. Bazant, Model for localization of softening and size effect, in: Inelastic Analysis of Structures, 2002 (Ch. 26).
[69] P.D. Washabaugh, W.G. Knauss, A reconciliation of dynamic crack velocity and Rayleigh wave speed in isotropic brittle solids, Int. J. Fract. 65 (2) (1994) 97–114, https://doi.org/10.1007/BF00032282.
[70] J.K. Zhou, L.M. Ge, Effect of strain rate and water-to-cement ratio on compressive mechanical behavior of cement mortar, J. Cent. South Univ. 22 (3) (2015) 1087–1095, https://doi.org/10.1007/s11771-015-2620-9.
[71] K. Ravi-Chandar, An experimental investigation into dynamic fracture: I Crack initiation and arrest, Int. J. Fract. 3 (4) (1984) 105–262, https://doi.org/10.1007/s00018-012-1041-2.
[72] S. Yetgin, O. Çavdar, A. Çavdar, The effects of the fiber contents on the mechanic properties of the adobes, Constr. Build. Mater. 22 (3) (2008) 222–227, https://doi.org/10.1016/j.conbuildmat.2006.08.022.
[73] M. O'Farrell, S. Wild, B.B. Sabir, Pore size distribution and compressive strength of waste clay brick mortar, Cem. Concr. Compos. 23 (1) (2001) 81–91, https://doi.org/10.1016/S0958-9465(00)00070-6.
[74] F. Parisi, D. Asprone, L. Fenu, A. Prota, Experimental characterization of Italian composite adobe bricks reinforced with straw fibers, Compos. Struct. 122 (2015) 300–307, https://doi.org/10.1016/j.compstruct.2014.11.060.
[75] S. Wang, M.H. Zhang, S.T. Quek, Mechanical behavior of fiber-reinforced high-strength concrete subjected to high strain-rate compressive loading, Constr. Build. Mater. 31 (2012) 1–11, https://doi.org/10.1016/j.conbuildmat.2011.12.083.
[76] G. Araya-Letelier, F.C. Antico, M. Carrasco, P. Rojas, C.M. García-Herrera, Effectiveness of new natural fibers on damage-mechanical performance of mortar, Constr. Build. Mater. 152 (2017) 672–682, https://doi.org/10.1016/j.conbuildmat.2017.07.072.
[77] D. Daviau-Desnoyers, J.-P. Charron, B. Massicotte, P. Rossi, J.-L. Tailhan, Characterization of macrocrack propagation under sustained loading in steel fibre reinforced concrete, Mater. Struct. 49 (3) (2016) 969–982, https://doi.org/10.1617/s11527-015-0552-3.
[78] F. Aymerich, L. Fenu, L. Francesconi, P. Meloni, Fracture behaviour of a fibre reinforced earthen material under static and impact flexural loading, Constr. Build. Mater. 109 (2016) 109–119, https://doi.org/10.1016/j.conbuildmat.2016.01.046.
[79] M.L. Parra-Saldivar, W. Batty, Thermal behaviour of adobe constructions, Build. Environ. 41 (12) (2006) 1892–1904, https://doi.org/10.1016/j.buildenv.2005.07.021.